ABSTRACT

RAMAKRISHNA, HARSHINI. Multiphase Biodegradable Scaffolds for Tissue Engineering a Tendon-Bone Junction. (Under the direction of Dr. Martin W. King)

Tendons play an important role in transferring stress between muscles and bones and in maintaining the stability of joints. Tears in the joints have poor healing capacity and the lesions are associated with cartilage degeneration. Therefore, strategies are needed to promote repair and long-term regeneration of such joints. The ultimate goal of this study is to develop a biodegradable scaffold for tendon-bone junction regeneration. As a first step to achieve this, polylactic acid (PLA) yarns were braided into tubular scaffolds and cultured with unique TGF-β Type II receptor-expressing joint progenitor cells under static conditions. The scaffolds were designed to mimic the natural mice tendon-bone junction in terms of its structure, mechanical and immunochemical properties. Two types of PLA yarns were used. Those with round fibers had a 25μm diameter, while those fibers with a 4 deep grooved (4DG) cross-section had a thickness of 45μm. Three different tubular scaffolds measuring about 2mm in diameter were braided on a Steeger 16-spindle braiding machine (Model K80/16-2008-SE) to mimic the tendon-bone junction by using these different yarns. The three different scaffold structures were: 1) PLA hollow tube using round fibers, 2) PLA hollow tube using grooved and round fibers, and 3) PLA multicomponent tube containing round fibers in the sheath and grooved core fibers inserted within the lumen. The biological and mechanical performance of the three scaffolds were evaluated, including cell viability and proliferation using an alamarBlue™ assay, cell attachment and migration using a laser scanning confocal microscopy (LSCM) with a live/dead stain, gene expression analysis by quantitative real time-PCR (polymerase chain reaction) at different time points and dynamic

tensile strength and initial Young's modulus using an Instron mechanical tester. The mechanical test results indicated that the three different braided scaffold structures provided a wide range of mechanical properties that mimic the components of tendon bone junctions. The results of the biological tests confirmed cell viability, active cell attachment and proliferation throughout all three scaffolds. The gene expression of scleraxis and tenomodulin for the sorted TGF-β Type II receptor expressing cells was upregulated by the presence of the scaffolds. The hollow scaffolds showed slightly higher gene expression than the scaffold with an internal core component. Furthermore, this study has also identified that the three proposed types of braided scaffolds with some improvement in their structures have the potential to be used as scaffolds for the regeneration of a tendon bone tissue junction.

Multiphase Biodegradable Scaffolds for Tissue Engineering a Tendon-Bone Junction

by
Harshini Ramakrishna

A thesis submitted to the Graduate Faculty of
North Carolina State University
in partial fulfillment of the
requirements for the degree of
Master of Science

Textile Engineering

Raleigh, North Carolina

2015

APPROVED BY:

_____	_____
Dr. Martin W. King Committee Chair	Dr. Robert Dennis
_____	_____
Dr. Wendy Krause	Dr. Susan Bernacki

DEDICATION

To my beloved parents

To my friends

To my advisor Dr. Martin W. King

BIOGRAPHY

Harshini Ramakrishna was born on 21st February, 1992 in Chennai, Tamil Nadu, India. She is the second daughter to her parents. She completed her high school from SBOA Hr. Sec. School in Chennai. She pursued her Bachelor's degree in Textile Technology in Alagappa Chettiar College of Technology, Anna University, Chennai. During her Bachelors, Harshini worked on internships at Meridian Apparels and Arunachala Spinning Mills in Tirupur, India. She received her B.Tech degree in May 2013.

Following her Bachelor's, Harshini applied to the Master's program in Textile Engineering at North Carolina State University. She is a member of the Society of Biomaterials, Student Chapter in NCSU. She is an active member and holds the position of Treasurer of the Textile Association of Graduate Students (TAGS) for 2 years from May 2014. She expects to receive her Master of Science degree in December 2015.

She has presented her graduate research work as a poster in the Graduate Students Research symposium at NC State University 2015 and also at the Annual Meeting of the Society for Biomaterials at Charlotte, NC 2015. She has also been awarded the prestigious FIDE International Chess Rating after she participated in the Asian Youth Chess Championship in 2005. During her free time, she likes a good game of chess or listens to music.

ACKNOWLEDGMENTS

I would like to sincerely thank Dr. Martin W. King who has been a constant support and a guiding force during the entire course of this project. He has been a great mentor and has helped throughout my stay here in NC State both professionally and personally. He has always been a source of inspiration for budding Textile Engineers like me and I take great pride in calling him my mentor.

I would also like to thank Dr. Robert Dennis, Dr. Wendy Krause and Dr. Susan Bernacki for agreeing to be a part of my advisory committee. They have always been encouraging and provided valuable inputs while I was working on this project. I would like to extend my special thanks to Dr. Anna Spagnoli, Professor and Woman's Board Chair, Department of Pediatrics at Rush University Medical Center. I am grateful to her and her group members Tieshi Li and Joseph Temple for allowing me to work in their laboratories to make this study a success. My sincere thanks to all the technicians and researchers who have helped me with my study: William Barnes, Tri Vu, Judy Elson and Dr. Eva Johannes. I would also like to thank all the members of Dr. Martin King's Biomedical Textiles Group for their constant support. I am especially thankful to Ting He and Yu Xie for helping me with my experimental work.

Last but certainly not the least, I would like to express my love and gratitude to my parents, Mr. Ramakrishnan and Mrs. Akila Ramakrishnan for their never ending support, love and encouragement. This paper is a result of their hard work and support. My special thanks also goes out to my friends at NC State who made me feel at home from day one and encouraged me to complete my Masters.

TABLE OF CONTENTS

LIST OF TABLES

LIST OF FIGURES

Chapter 1

Introduction

1.1 Motivation and Significance

The tendon bone junction is a functionally graded material which helps in transition from a soft unmineralized tendon tissue to hard mineralized bone. It also plays an important role in transferring stresses and in maintaining the stability of joints. Tears in the joints have poor healing capacity and the lesions are associated with cartilage degeneration. The most common tendon bone junction injuries are the achilles tendon injury, rotator cuff injury and anterior cruciate ligament (ACL) injury. Studies indicate that every year there are about 100,000 ACL reconstruction surgeries, 75,000 rotator cuff repairs and 230,000 Achilles tendon repairs performed in the United States.

Generally the tendons are restored successfully but the functional graded transitional tendon bone interface is not regenerated. Thus, one of the most immediate challenges facing the field of regenerative medicine is "Interfacial Tissue Engineering" (ITE), which addresses the question of how to generate a multiple tissue junction such as a tendon/bone interface which has integrity, continuity and consists of two or more different yet contiguous types of cells. Up until now ITE has taken the approach that it is necessary to use pluripotent stem cells or to co-culture the two dissimilar cell lines either in sequence, one after the other, or together in a single compromised media and co-culture condition. This approach assumes that a tissue junction consists of only two types of tissue that are joined at the interface.

Many previous developmental-stage studies on mouse embryos have shown evidence of a distinct intermediate interfacial tissue type, for example between the bone and the tendon.

Our approach is to focus on the unique joint TGF-βType II receptor-expressing progenitor cells that have shown to have *in vivo* and *in vitro* anatomical, ontogenic and slow-cycling expression profiles of progenitor joint cells [45, 46]. By applying these unique cells to multiphase tissue engineering scaffolds that contain a continuous gradient between two different but contiguous structures, one mimicking the architecture, porosity, mechanical and immunochemical properties of the tendon, and the other mimicking bone tissue, we anticipate developing a new approach to bone/tendon ITE without the use of pluripotent stem cells or the need to co-culture two or more different cell lines. In order to develop the multiphase tissue engineering scaffolds, we are proposing to use braiding technology. Braiding technology uses a given number of yarns to intertwine or braid them into a tubular structure. For many years this has been used to manufacture ropes, cords and shoe laces and now it is being used in other fields such as medical textiles.

1.2 Goals and Hypothesis

The ultimate goal of this study is to fabricate and evaluate the properties of our specially designed biodegradable multiphase scaffolds braided from poly(lactic acid) (PLA) yarns. However, before reaching the ultimate goal the main objective and hypothesis is to demonstrate that our specially designed biodegradable multiphase scaffolds braided from poly(lactic acid) (PLA) yarns can support the attachment, viability, proliferation and gene expression of murine TGF β Type II receptor-expressing joint progenitor cells.

There are three specific aims:

1. To design and fabricate biodegradable multiphase scaffolds braided from poly(lactic acid) (PLA) yarn with the appropriate braiding angle. The design was to use filaments with both a grooved and a round fiber cross-section, and to include of a core yarn within the circular braid so as to mimic the dynamic mechanical properties of the natural mouse tendon and bone regions before and after cell culture. Three different types of scaffolds were fabricated in this study. They were:
    i. PLA hollow tubes using round fibers
    ii. PLA hollow tubes using grooved and round fibers (grooved fibers promote cell attachment and alignment) and
    iii. PLA bilayer tubes with round fibers and grooved fiber insertion (mimicking the bone region).
2. To evaluate the structure and mechanical properties of the three different types of scaffolds and compare the performance of the scaffolds with respect to using a grooved instead of a round fiber cross-section and the inclusion of a core yarn within the circular braid. The study includes the following tests:
    i. To evaluate the morphology of the three different kinds of scaffolds and to measure their porosity.
    ii. To perform mechanical tests to find out the tensile strength, elongation at break and initial modulus of the three different specially designed biodegradable multiphase scaffolds.

iii. To analyze any differences between the three different scaffolds using statistical analysis.

3. To determine how the gradient in the design of the PLA scaffold structure which mimicked the tendon and bone tissues, effects the attachment, viability, proliferation and gene expression of murine TGF-β Type II receptor-expressing joint progenitor cells under static culture conditions. The study includes the following tests:

   i. To evaluate the biological performance of the three different types of scaffolds cultured with murine TGF β Type II receptor-expressing joint progenitor cells and testing it at different time points. All the three samples were coated with serum before cell culture. The alamarBlue^{TM} assay was used to evaluate the cell viability and cell proliferation on the three different types of scaffold. The migration and attachment of cells along the surface and internal structure of the three different scaffolds were observed by laser scanning confocal microscopy (LSCM). In order to visualize and differentiate the live cells from the dead cells, Live/Dead cell double staining kit was used. Quantitative polymerase chain reaction (qPCR) was used to detect the gene expression of two important tendon proteins namely scleraxis and tenomodulin.

   ii. To compare the biological performance of the three different types of scaffolds and analyze any differences between them using statistical analysis.

According to the objectives, I hypothesize that:

1. The use of a braiding technique will help us get a desirable range of pore sizes that will prevent leaking of cells into the hollow luminal space of the tubular scaffold. The loss of cells could lead to a decrease in cell interaction which in turn could affect cell differentiation.
2. It also protects the multiphase scaffold from structural changes during the process of heat setting which is done to maintain the dimensional stability of the scaffolds in the liquid culture media.
3. The insertion of core fibers inside the hollow braided structure will improve the dimensional stability and mechanical strength of the scaffold which in turn will mimic the natural mouse bone structure.
4. The incorporation of grooved 4DG PLA fibers will improve the attachment, proliferation and penetration of the murine TGF β Type II receptor-expressing joint progenitor cells on the specially designed biodegradable multiphase scaffold.

1.3 Outline of the Thesis

This thesis is organized into five chapters. The first chapter describes the motivation and significance of this particular research in the regeneration of tendon bone tissue junctions. It also lists the specific aims and objectives of the study. The second chapter reviews the important literature that describes the structure and composition of tendon bone junctions, injuries associated with tendon bone junction and current surgical repair techniques. The selected materials for this study are highlighted and discussed in detail. The third chapter describes the experimental design including the materials, fabrication methods and methods

used to test the biological and mechanical properties of the scaffolds. The fourth chapter reports the results, and includes a discussion of the findings from the characterization of the three different types of multiphase scaffolds as well as their mechanical and biological performance. Lastly, the fifth chapter gives a summary of the findings, conclusions and recommendations for future work.

Chapter 2

Review of Literature

2.1 Structure and Properties of Tendon Bone Junction

Tendons are connective tissues that connect muscles to bones and form a musculotendinous tissue whose primary function is to transmit tensile load and stabilize joints. A tendon is defined as a dense highly organized tissue that transmits an applied force and is composed predominantly of type 1 collagen with fibril associated proteoglycans. According to evolutionary history, the first tendinous tissue appeared in the invertebrate chordate Branchiostoma as myosepta. In myosepta the collagen structure was highly organized with fibers running along two primary axes [1].

In humans, tendons have a multi-unit hierarchical structure composed of collagen molecules, fibrils, fiber bundles, fascicles and tendon units that run parallel to the tendon's longitudinal axis (Figure 2.1). The smallest structural unit of a tendon is the fibril. It is made up of rod like collagen molecules aligned end to end in a quarter staggered array. The diameter of the collagen fibril varies from 10 to 500nm and depends on the age, sample location and species of the host. Fibrils are followed by fibers. Collagen fibers contain collagen fibrils and are bound together by endotenons, thin layers of connective tissue containing capillaries, lymphatic vessels and nerves. Fascicles are made up of fiber bundles, and the bundles of fascicles are covered by epitenon, a fine loosely connective tissue sheath containing the vascular and lymphatic vessels and the nerve supply to the tendon. Tendons are also enclosed by a third layer of connective tissue known as the paratenon, or synovial sheath. The combination of epitenon and paratenon is known as the peritendon which reduces the friction

with adjacent tissues. This hierarchical structure of the fiber bundle contributes to the tensile strength of the tendon [2].

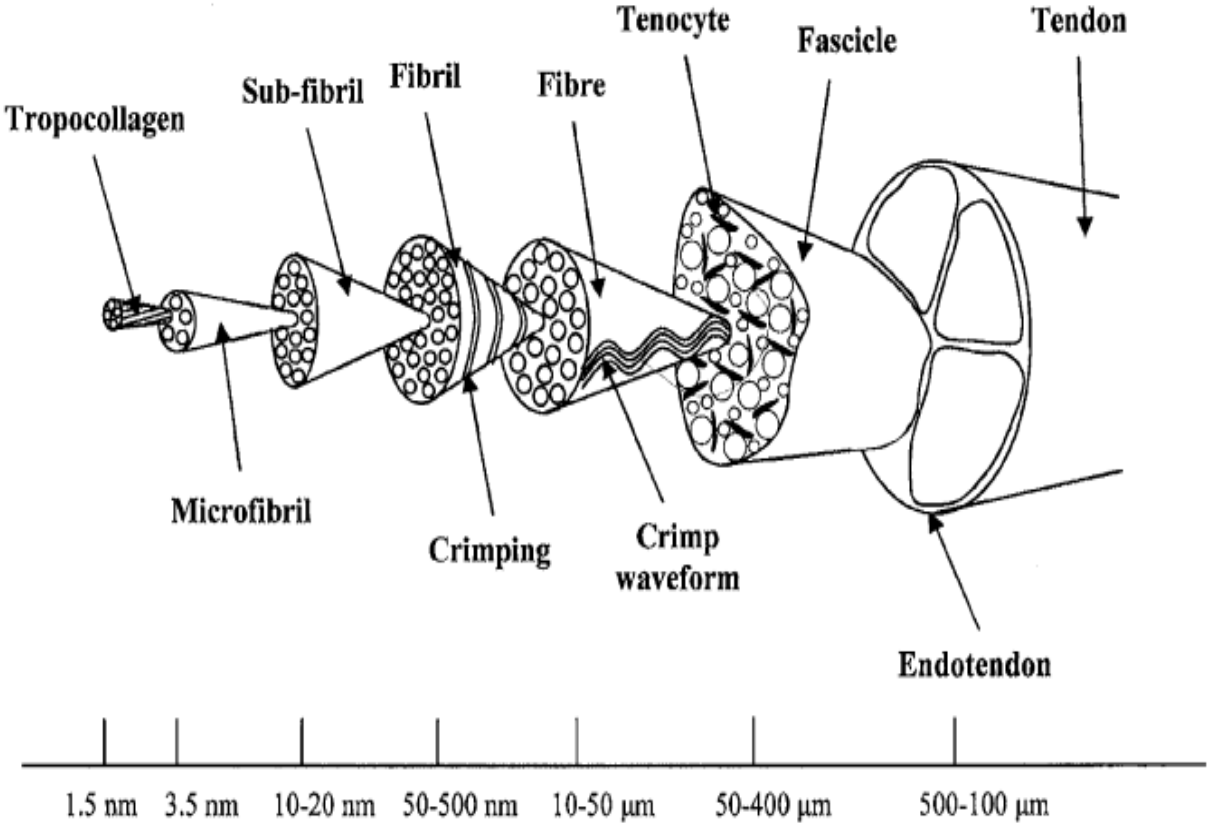

Figure 2.1 Hierarchical structure of a tendon structure containing collagen molecules, fibrils, fiber bundles, fascicles and tendon units that run parallel to the tendon's longitudinal axis [3]

The composition of a tendon consists of 86% collagens, 1-5% proteoglycans, 2% glycoproteins and 60-80% water. It contains relatively few cells, with the predominant cell type being the fibroblast [4]. In tendons, type I collagen constitutes about 95% of the total collagen content and the remaining 5% consists of types III and V collagens. Tropocollagen, a long thin protein is the basic structural unit of collagen. It is produced inside the cell and

released into the extracellular matrix as procollagen, which has a non-triple helical extension at both ends [5]. Type III collagen is mainly found in the endotenon and epitenon where it forms smaller, less organized fibrils that result in decreased mechanical strength. Type V collagen is inserted into the core of type I collagen fibrils to regulate fibril growth. Collagen types II, VI, IX, X and XI are found in trace amounts at the bone insertion site of fibrocartilage. They strengthen the tendon bone connection by reducing the stress concentration at the hard tissue interface. The collagens found in the matrix are cross linked to increase the Young's modulus of the tendon and reduce the level of strain at failure.

Besides collagen, tendons also contain a variety of proteoglycans (PGs) such as decorin, biglycan, fibromodulin, lumican, epiphycan and keratocan [5,7]. The proteoglycan content of a tendon varies depending on its mechanical loading condition. Decorin is a small leucine rich proteoglycan which is located on the surface of the middle portion of collagen fibrils. It facilitates fibrillar slippage during mechanical deformation and also assists the collagen molecules to align within the tendonous structure. The other proteoglycans present in tendons help in holding water within the fibrocartilage and resist compression. Glycoproteins such as tenascin-C and fibronectin are also present in the extracellular matrix (ECM) of the tendon. Tenasin-C contributes to the mechanical stability of the extra cellular matrix whereas fibronectin facilitates wound healing.

Tendons consist of endothelial cells, synovial cells, chrondrocytes and fibroblasts. The most dominant cell type is the fibroblast which is responsible for synthesizing extracellular matrix proteins, producing an organized collagen matrix and remodeling it during tendon healing [2].

The fiber morphology and viscoelastic behavior of the tendon are responsible for its unique mechanical behavior when subjected to dynamic stress in vivo. A typical tendon stress-strain curve is shown in Figure 2.2. It has an initial toe region where the tendon is strained up to 2%, which corresponds to the stretching–out of the "crimp pattern" of a tendon. The initial toe region is followed by a linear region where the tendon is stretched up to 4% and the collagen fibers lose their crimp morphology. The slope of this recoverable region is known as the Young's modulus. If the tendon is stretched beyond this the linear region, that is more than 4%, microscopic tearing occurs in the tendon fibers and further stretching results in macroscopic failure and tendon rupture.

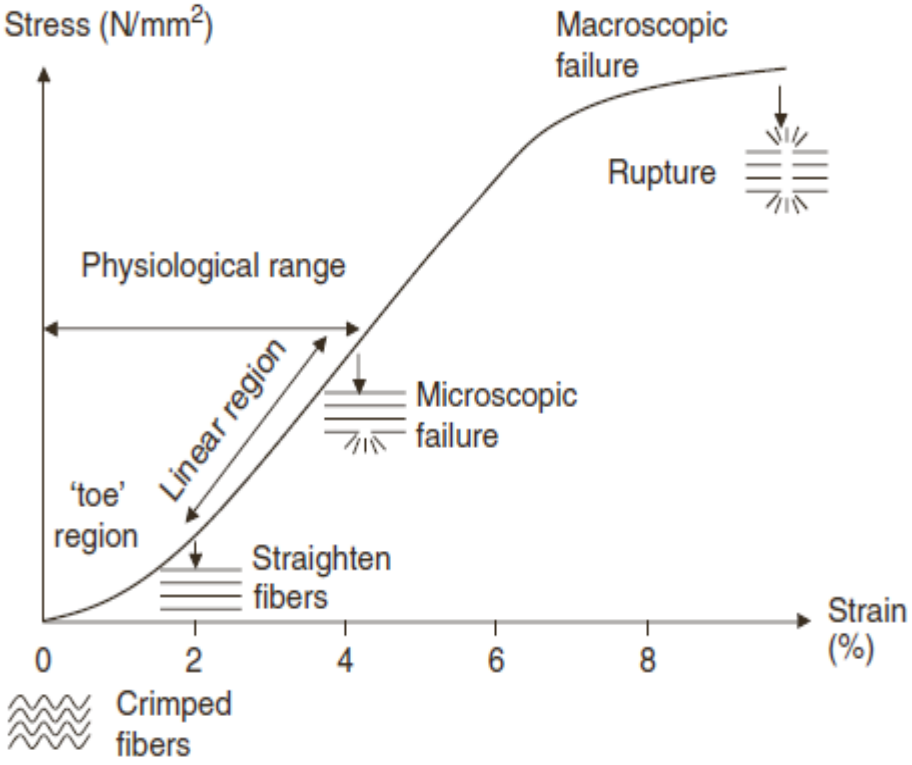

Figure 2.2 Stress strain curve of a tendon [2]

When tendons are injured, the body initiates a process of healing and scar formation. Although the tensile strength of a healing tendon improves over time, it never reaches the level of normal, healthy uninjured tissue due to its hypocellular and hypovascular nature [7]. The healing capacity of a tendon is poor. Following injury the biochemical and ultrastructural characteristics remain abnormal even after 12 months due to its high *in vivo* loading, the Achilles tendon is the most frequently injured tendon in the human body, followed by the patellar tendon. Tishya et al., [6] studied the mechanical properties of the human Achilles tendon and found that its mechanical performance depends on the strain rate even though its material properties are similar to other tendons.

Tendons attach to bone through an insertion site known as an enthesis. The plural is enthuses. The insertion site is also known as an osteotendinous junction. The enthesis connects two vastly different, highly ordered hierarchical tissues across a millimeter wide junction region. The enthesis can further be divided into two types depending on the type of tissue present at the skeletal attachment site. It can either be fibrous connective tissue or fibrocartilage. A fibrous enthesis attaches directly to the bone or periosteum via fibrous tissue which is similar to a mid-tendon region, whereas a fibrocartilage enthesis attaches to bone through a layer of fibrocartilage which acts as a transition zone between the bone and the fibrous tendon tissue [8,9]. The majority of entheses in the body are fibrocartilaginous and they are more frequently injured. Thus they are more commonly studied. The main characteristics of fibrous and fibrocartilaginous entheses are shown in Table 2.1.

Table 2.1 Characteristics of fibrous and fibrocartilaginous enthesis [8]

	Fibrous Enthesis	**Fibrocartilaginous Enthesis**
Common attachment	Metaphyses and diaphysis of long bones	Epiphyses and Apophyses
Composition	Mineralized collagen fibers	Four distinct zones
Angle of insertion	Insertion angle changes slightly during motions	Prone to overuse injuries as changes in the insertion angle are greater
Example	Deltoid attachment to the humerus and adductor magnus to the lineaaspera of the femur, pronator teres	Rotator cuff and Achilles tendons

Fibrous entheses are typically found attached to larger boney surface areas and are distinguished by the presence of mineralized collagen fibers. These entheses can either be boney or periosteal, depending on whether the tendon attaches directly to the bone or the periosteum. It is distinguished by the presence of dense fibrous connective tissue at the tendon-bone interface and such structures are common in tendons that attach to the diaphysis of long bones. For example, this type of enthesis is found in muscles which are connected to the humerus and muscles which are attached to the linea aspera of the femur [8, 10].

Fibrocartilaginous entheses are distinguished by the presence of a fibrocartilage transition zone at the tendon bone interface. They are more common and are prone to overuse injuries

such as those of the rotator cuff and Achilles tendon. These enthuses have been categorized into four zones (Figure 2.3) to form a structurally continuous gradient from the flexible uncalcified tendon to the rigid calcified bone [18,19].

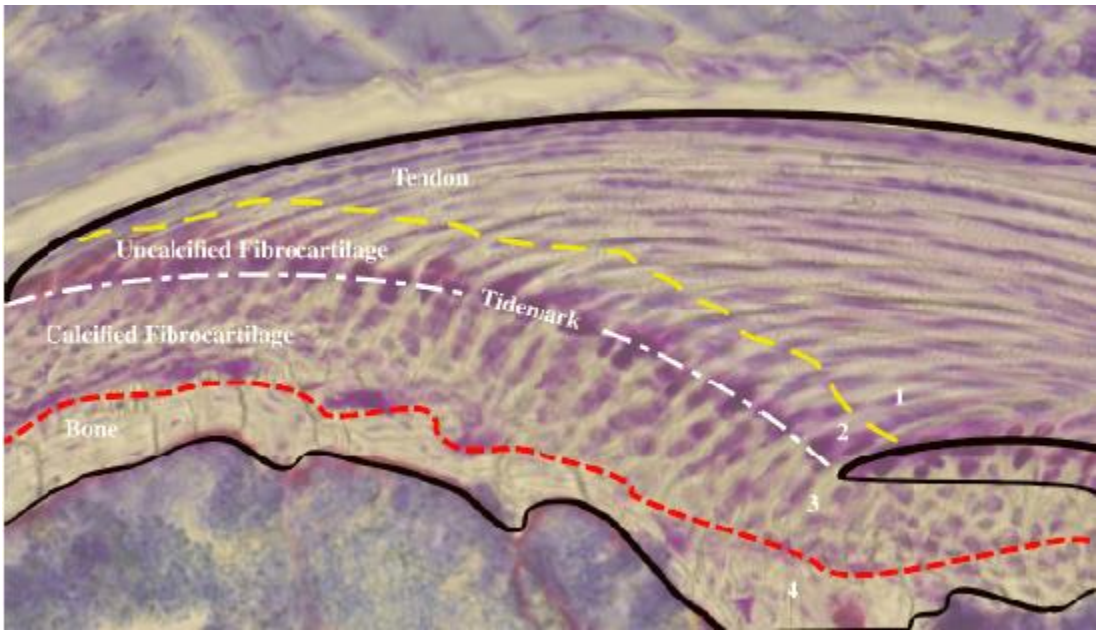

Figure 2.3 The four zones of the enthesis viewed in a histological section: Zone 1-Pure dense fibrous connective tissue, Zone 2-Uncalcified fibrocartilage, Zone 3-Calcified fibrocartilage, Zone 4-Bone [8]

The first zone is the pure dense fibrous connective tissue. It consists of pure tendon and its properties are similar to the mid-substance tendon and it is heavily populated by fibroblasts. It also consists of linearly aligned type 1 collagen and trace amounts of type III collagen, elastin and proteoglycan decorin. The second zone is the uncalcified fibrocartilage and it marks the beginning of the transition from flexible tendinous material to rigid bony material. It consists of fibrochondrocytes, collagen types II and III and small amounts of types I, IX and X collagen and proteoglycans, aggrecan and decorin. The function of this zone is to

dissipate the bending of collagen fibers in the tendon. The “tide mark” is a mechanical boundary or basophilic line separating the uncalcified soft tissue from the calcified hard fibrocartilage zone. It is relatively straight indicating the production of a flat surface during mineralization. The third zone is the calcified fibrocartilage zone. It is an avascular zone of calcified or mineralized fibrocartilage containing fibrochondrocytes indicating a marked transition towards bony tissue. Type II collagen is predominantly found in this zone and types I and X collagen as well as aggrecan is found in trace amounts. In contrast to the tidemark, this junction is highly irregular and it provides the mechanical integrity of the enthesis. This layer allows a gradual transition of force across the enthesis and it also acts as a barrier against blood vessels in the bone. Thus preventing direct cell-cell communication between osteocytes and tendon cells. The fourth and the final zone is the bone itself. This zone has a high mineral content. It consists of osteoclasts, osteocytes and osteoblasts residing in a matrix of type I collagen and carbonized mineral [8,11]. The composition and significance of the four zones is summarized in the Table 2.2.

Table 2.2 Composition and significance of the four zones of an enthesis [8]

	Composition	**Significance**
Zone 1 Pure dense fibrous connective tissue	Fibroblasts, Type I collagen, Type III collagen	Linearly arranged collagen with mechanical properties similar to central region of tendon
Zone 2 Uncalcified fibrocartilage	Fibrochondrocytes, Proteoglycan aggrecan with collagen (Types I and III)	Dissipates bending of collagen fibers in tendon
Tidemark		Basophilic demarcation between uncalcified and calcified fibrocartilage representing the boundary between soft and hard tissues
Zone 3 Calcified Fibrocartilage	Fibrochondrocytes, predominantly Type II collagen, Type I and Type X collagen	Irregularity of attachments into bone give mechanical integrity of enthesis
Zone 4 Bone	Osteocytes, Osteoblasts, Osteoclasts, Type I collagen	Provides sites of attachment for the tendon

The tendon to bone insertion is a biomechanically, compositionally and structurally complex junction. The insertion site has to transfer a complex loading environment effectively to prevent injury. So it is believed that the properties of the insertion site vary along its length. In order to demonstrate this, Stavros et al., [12] used a quasilinear viscoelastic model to

determine the biochemical properties, polarized light analysis to determine the collagen orientation and *in situ* hybridization to determine the expression of cellular matrix genes. It was found that there was a variation in gene expression along the length of the insertion. Tendon specific genes such as decorin and biglycan were present only on the tendon end of the insertion, whereas cartilage specific genes such as collagen II and aggrecan were present only at the bony end of the insertion. It was also found that the collagen fibers were less oriented near the insertion points compared to the tendon.

Andrew et al., [13] compared the extracellular matrix in the middle of the tendon with the extracellular matrix near the insertion region using immunohistochemical analysis. He found that there is a striking difference between the ECM found in these two regions. Many experiments have been conducted to establish how a contiguous tendon bone insertion derives its mechanical properties [14, 15, 16]. They found that there are two main factors that contribute to the tendon to bone transition with its unique gradient in mechanical properties. One is the gradient in mineral concentration and other is the gradient in collagen fiber orientation. The insertion zone was significantly stiffer at the tendon end compared to the bony end, and it was also found that mineral deposits accumulate within the collagen fibers provided stiffening of the mineralized fibers. Thus it appears that the tendon to bone insertion site varies along its length with respect to collagen structure, extracellular matrix composition, mineral content, geometry and viscoelastic properties. This variation distributes the applied forces effectively across the transition from a flexible tendon to a rigid bone.

Since an enthesis attaches a soft tendon material to a stiff bone, it has the tendency to generate a high stress concentration which might result in overuse injuries. This is

particularly common in sports [9]. Surgical reattachment often fails due to the poor healing of the enthesis. Pauline et al., [17] reported that about 20-90% of rotator cuff repairs failed and the failure rate of ACL reconstruction ranged between 10 to 20%. The poor healing of the enthesis is due to several factors including poor vascularization within the fibrocartilage zone, mechanical loading, extracellular matrix composition as well as other biological factors.

2.2. Tendon Bone Junction Injuries

The tendon bone junction is a material with a structural gradient, which provides a functional transition from soft unmineralized tendon tissue to hard mineralized bone. Due to its unique mechanical behavior there is a possibility of accumulating unwanted stress at the interface, which results in injury. Below are a few examples of tendon bone insertion zones that are frequently injured, are slow to heal and difficult to repair surgically.

The rotator cuff is a group of tendons and muscles in the shoulder which connects the bone in the upper arm (humerus) to the shoulder blade scapula. The rotator cuff tendons and muscle provide stability and limit the extent of motion in the glenohumeral joint. There are four different muscles in the rotator cuff which are the teres minor, the infraspinatus, the supraspinatus and the subscapularis. Each muscle has an insertion point at the scapula and has a tendon that attaches to the humerus. The tendons and tissues together form a cuff around the humerus. A rotator cuff injury occurs when these tendons are torn or separated from the humeral head which then leads to loss of function, instability and pain. About 30% of the population over 60 years of age has a rotator cuff tear and orthopedic surgery is the normal operation performed to recover shoulder function. In fact there are about 75,000

rotator cuff repairs performed each year in the United States [20].Generally the tendons are reattached successfully but the functional transitional gradient at the tendon bone interface is not regenerated. This leads to one of the most important challenges in clinical practice in which the incidence of repeat rotator cuff failure is between 30 to 94%. Figure 2.4 shows the cross-sectional view of a mouse supraspinatus tendon-to-bone insertion. The collagen fiber orientation becomes less well aligned as the tissue extends from tendon to bone [20].

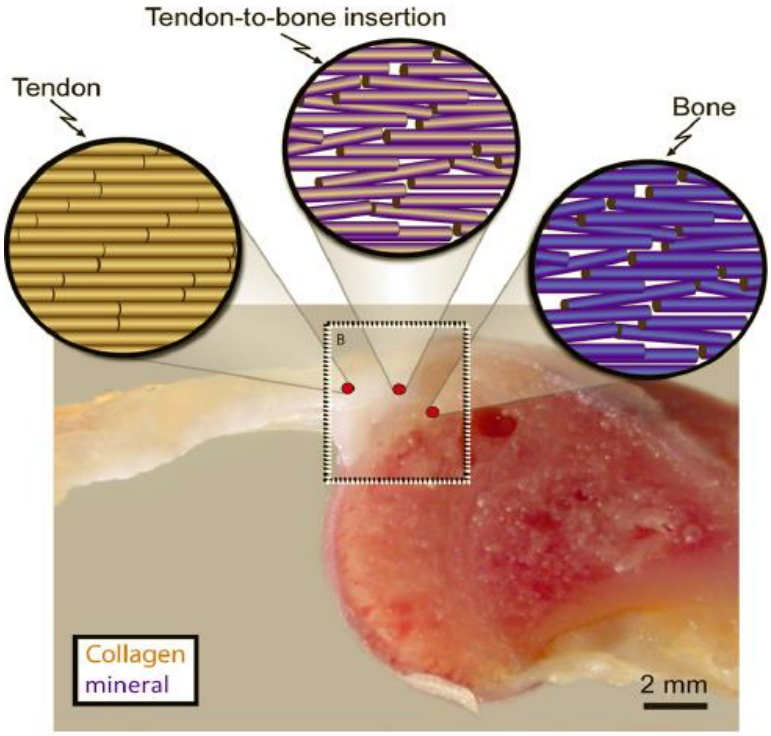

Figure 2.4 Cross-sectional view of a mouse supraspinatus tendon-to-bone insertion where yellow color indicates collagen and blue indicates mineral content [20]

The Achilles tendon is a fibrous tissue which connects the heel bone (calcaneus) to the calf muscles gastrocnemius and soleus muscles (Figure 2.5). It is the largest and strongest tendon found in the human body, and that is why orthopedic surgeons will harvest part of a patients Achilles tendon to serve as autologous donor tissue to repair an injured tendon on ligament elsewhere in the body. The Achilles tendon is also the most commonly injured tendon. Injury may be due to overuse or too much physical activity, misalignment, improper footwear, medication side effects and/or accidents. It is most common among athletes who participate in sports involving maximum effort, which invariably leads to excessive applied loads and/or levels of strain. Studies indicate that about 230,000 Achilles tendon injuries occur each year in the United States [21]. Regeneration of a well attached tendon bone interface is a challenge, due to poor healing of the enthesis.

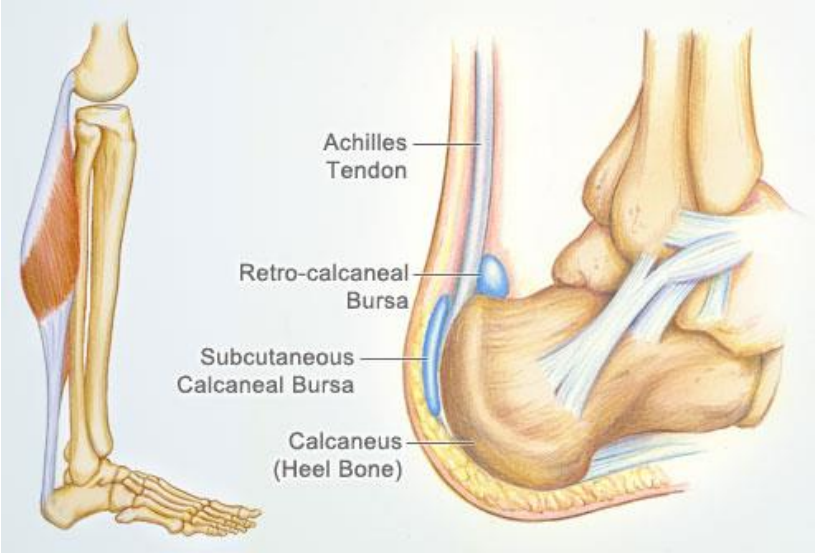

Figure 2.5 Structure of Achilles tendon [21]

The next most common type of bone junction injury is the anterior cruciate ligament (ACL) tear. The ACL is one of a pair of cruciate ligaments in the human knee located behind the knee cap (the patella). It originates from the medial and anterior aspect of the tibial plateau and runs towards its insertion point on the lateral femoral condyle (Figure 2.6). Approximately 100,000 ACL reconstructive surgery operations take place each year in the United States [20]. It is also common among the athletes who are likely to experience frontal impacts, such as in football and downhill skiing. Autografts and allografts are used to repair ACL injuries. The most common method is to take bone-tendon-bone tissue from the patellotibial junction of the uninjured knee and to reattach it at the injured site. This method facilitates bone to bone integration by placing the auto graft within the lumen of the bone tunnels, but graft harvesting damages the healthy donor site resulting in patient morbidity, chronic joint pain and osteoarthritis. Another common procedure for repairing an ACL tear involves the fixation of the hamstring or gracilis tendon between the tibia and femur. This minimizes donor site complications but has other disadvantages, such as graft slippage or graft impingement. The other limitations of using the above methods are graft availability, the need for sterilization, the risk of transmitting donor pathogens and reduced biological and mechanical integrity [20].Thus the limitations of the existing methods for the repair of tendon/ligament to bone insertion motivates the need for new cell and biomaterial based therapies.

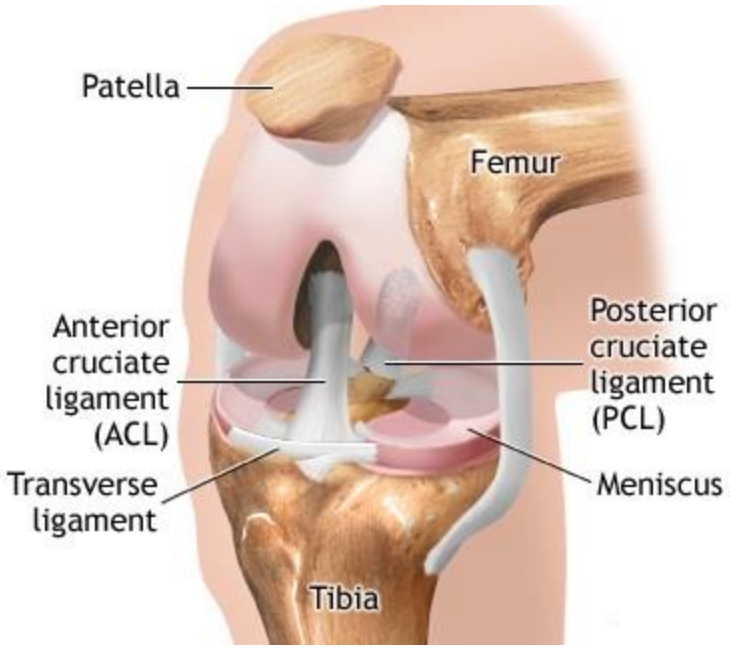

Figure 2.6 Anatomical location of an anterior cruciate ligament [22]

2.3 Strategies for the Repair and Regeneration of Tendon Bone Junctions

There are many challenges in repairing and regenerating tendon to bone junctions. Liu at al [26] tried to simulate a numerical model for the tendon bone insertion, through numerical optimization of a mathematical model. Optimizations were carried out on a rotator cuff insertion site model and they showed that the stress concentration can be reduced by a biomimetic gradient of material properties. It was noted that the scar tissue produced by routine surgical techniques is not effective in reducing the stress concentration.

There are three main issues that need to be addressed while mimicking the tendon bone junction. First the tendon bone insertion site must be mechanically stable during healing. Second, the structure must generate a natural, gradient tissue. Finally the tissue engineered scaffold structure must support an organized multicomponent system where spatially variable

populations of cells are sustained so as to produce structural and mechanical gradients. Figure 2.7 demonstrates the anatomy of a tendon bone insertion that must be achieved by a successful tissue engineered construct.

Figure 2.7 Anatomy of tendon bone insertion showing the four zones: tendon, uncalcified fibrocartilage, calcified fibrocartilage and bone [25]

One strategy for repairing the tendon bone junction is to use stratified constructs [20, 23]. Here each biomaterial stratum is seeded with its own individual cell type appropriate for that region of the insertion and the strata are held together in the required sequence. It is believed that having multiple phenotypes in proximity to each other will result in the formation of a graded insertion site (Figure 2.8).

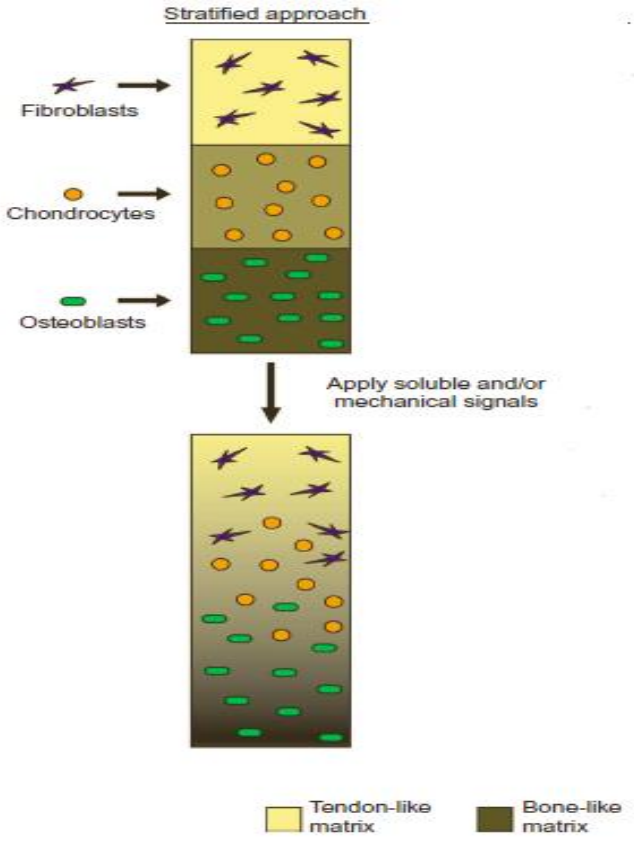

Figure 2.8 Stratified approach strategy [20]

Spalazzi et al., [24] designed a multiphase scaffold: Phase A was fabricated from sheets of a polyglactin knitted mesh, Phase B from PLGA microsphere and Phase C consisted of composite microspheres with a 4:1 ratio of PLGA and bioactive glass. Bovine fibroblasts and

osteoblasts were seeded on either end of the scaffold leaving the central region for the formation of the enthesis. Both fibroblasts and osteoblasts migrated into the central zone and there was significant Type I collagen deposition in both the central region and the zone seeded with fibroblasts. The end zone seeded with osteoblasts had significant mineral deposition while tendon-like and bone-like structures were formed in the extreme end zone, a transition insertion region with the generation of fibrocartilage was not achieved in the central zone [25]. In order to produce a fibrocartilagenous central zone, it was found necessary to seed chondrocytes. Thus by using three cell populations, three separate but contiguous zones of tendon-like, fibrocartilagenous and bone-like structures were achieved (Figure 2.9).

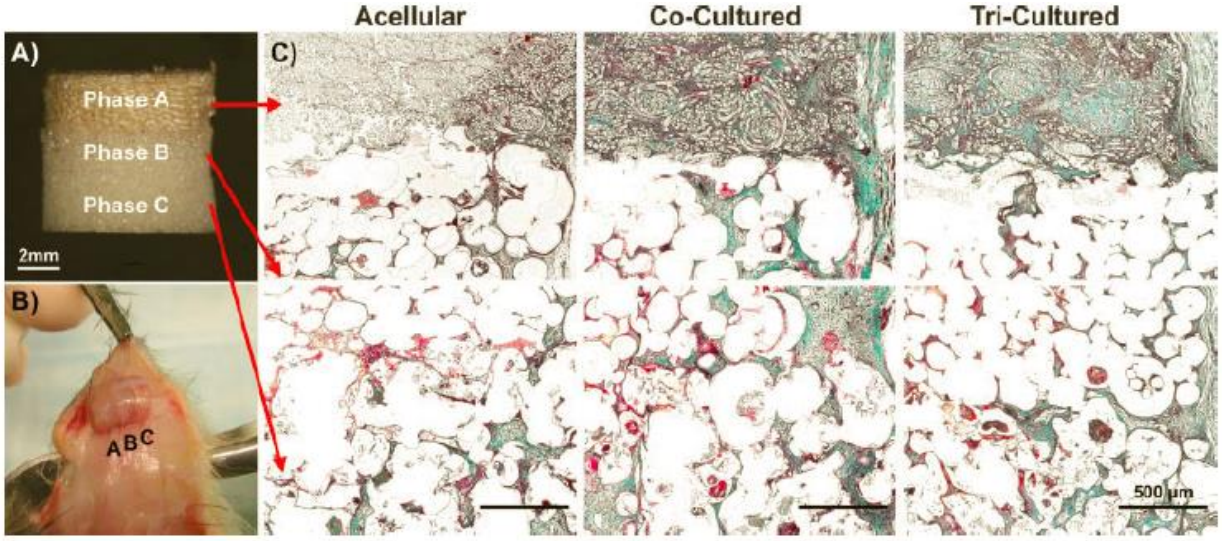

Figure 2.9 (A) Triphasic scaffold with three distinct yet contiguous phases (B) Explanted tri-cultured scaffold at Week 4. (C) Collagen production (green) on the dorsal side of the acellular, co-cultured and tri-cultured scaffolds after 4 weeks of implantation [24]

In another approach a composite system was created using PLGA nanofibers and hydroxyapatite nanoparticles and the scaffold was seeded with fibroblasts, chondrocytes and osteoblasts. The experimental results indicated that the three cell populations showed promising proliferation on the polymer ceramic composite nanofibers [23]. However seeding three multiple cell types onto a stratified tissue composite had its limitations. Cost is a major concern, and there are practical challenges for clinical use since it involves isolating mature fibroblasts, chondrocytes and osteoblasts from three separate sites. There is another approach which utilizes a single pluripotent mesenchymal stem cell which can differentiate into multiple mesenchymal tissues [32]. It is believed that a combination of biochemical and mechanical stimuli will promote cell differentiation resulting in a tissue gradient. Utilization of mesenchymal stem cells was compared with the injection of chondrocytes for the regeneration of a tendon bone junction [31]. It was found that the mesenchymal stem cell treatment developed a stronger tendon bone junction than the chondrocyte treatment. In fact the morphological and biomechanical characteristics of the regenerated tendon bone junction were similar to those in a natural human tendon bone junction. More recently Shahab et al., [28] has found that viral modification of mesenchymal stem cells is able to enhance the formation of a fibrous tendon bone junction. The tenogenic and osteo/chondrogenic characteristics are developed by the adeno and lentiviral expression of the biologically active Smad8 signaling mediator and bone morphogenetic protein 2 (BMP2).

The periosteum contains multipotent mesodermal stem cells that have the ability to differentiate into both osteogenic and chondrogenic tissues. A biomechanical and histological study of the periosteum in rabbits has demonstrated that mesodermal stem cells have the

ability to enhance the healing of a tendon bone interface, and has suggested that these cells can be placed on the torn end of an injured tendon to enhance tendon bone junction healing [33]. Kartogenin (KGN), a natural biopolymer, has also been found to improve the healing of injured tendon bone junctions [29]. It promotes the formation of cartilage-like tissue at the tendon bone interface.

Hepatocyte growth factor is also an active compound in its heterodimeric form. It has the ability to couple with the Met receptor in the target cells and promote cell proliferation, migration and the induction of morphogenesis. It also induces the expression of the receptor for bone morphogenetic protein (BMP). Junsuke et al., [30] studied the effect of hepatocyte growth factor (HGF) in a rabbit tendon bone healing model. Histological analysis showed that the HGF treated rabbit group had better biomechanical properties and enhanced tendon bone junction healing.

Fibroblast growth factor (FGF) is another growth factor which promotes tendon bone junction healing. Histological studies [35] have shown that the application of FGF-2 accelerates the tendon bone healing in rats. It plays a critical role in angiogenesis and mesenchymal cell mitogenesis. It also has the ability to induce transforming growth factor β (TGF-β) gene expression and by increasing the release of TGF-β and bone morphogenic protein (BMP) it can initiate the growth of bone at a tendon bone junction. TGF-β signaling has the potential to induce tendon progenitor marker scleraxis. Spagnoli et al., developed a transgenic mice Tgfbr2-β-Gal-GFP-BAC using mouse bacterial-artificial-chromosome (BAC) clone RP24-317C21 containing the TGF-β type II receptor and a GFP-IRES-β-GAL-GEO cassette was inserted into the TGF-β type II receptor-BAC at the endogenous TGF-β

type II receptor translational start site to have β-Gal and GFP as imaging reporters for TGF-β type II receptor expression under the control of the promoter and endogenous TGF-β type II receptor gene regulatory sequences. It has been found that TGF-β type II receptor expressing cells play an important role in embryonic joint development and by inactivating this signal in rats, it has been shown to lead to the absence of interphalangeal joint development [45, 46]. It was also identified that TGF-β type II receptor is highly and specifically expressed in developing joints.

Chen et al., [27] developed an injectable hydrogel made of periosteal progenitor cells and poly(ethylene glycol) diacrylate tethered to bone morphogenic protein-2 to enhance the healing of a tendon bone junction. BMPs are multifunctional cytokines which belong to the transforming growth factor-beta (TGF-β) family and function as an important positive regulator of osteoblast differentiation. The hydrogel was injected into rabbits and the morphological characteristics of the tendon bone junction were evaluated by histology and immunohistochemical techniques. In addition, biomechanical tests were also undertaken so as to determine the strength of the tissue junction. The tests were performed at 4 and 8 weeks. The results from histology and immunohistochemical analysis showed the formation of collagen fibers, fibrocartilage and a layer of bone located at the tendon bone junction. It also showed the presence of aggrecan. Biomechanical testing confirmed that the strength of the interface increased with time. From this it was concluded that the hydrogel design successfully enhanced the process of tendon-bone healing. In another study to develop a functional tendon bone junction, Yusuke et al., [34] injected recombinant human bone

morphogenetic protein 2 into a rabbit tendon. This led to the formation of an ossicle, and the tendon/ossicle complex eventually developed a stable tendon bone junction.

An enamel matrix derivative is an extract that has been derived from dental bacteria on the teeth of six month old pigs and is composed of several different proteins such as amelogenin, enamelin, seathlin and proteases. It is believed that this enamel matrix derivative promotes regeneration of soft and hard tissues surrounding the teeth. Because these tissues have a slow rate of healing much like a tendon bone junction, Kadonishi et al., [36] hypothesized that the application of this enamel matrix derivative to the tendon bone junction might promote the rate of regeneration. Emdogain® is a commercially available enamel matrix derivative composed of porcine enamel matrix derivative and propylene glycol alginate. Kadonishi introduced Emdogain® into the flexor digitorum tendons of 30 Sprague Dawley rats and then performed histological analysis and biomechanical testing after eight weeks. The Emdogain® treated rats showed greater collagen fiber production as well as increased biomechanical strength at the tendon bone junction. From this it was concluded that enamel matrix derivative assists in the regeneration and repair of tendon bone junction.

A more recent method for the treatment of injured tendon bone junctions is the use of a three dimensional biodegradable scaffolds. The scaffolds must be biocompatible, highly porous and biodegradable. It should also promote cell attachment, proliferation and differentiation and recruit fibroblasts that can secrete their own extracellular matrix resulting in the generation of living tissue. Yokoya et al., [37] compared three synthetic polymers: polytetrafluoroethylene (PTFE), poly-L-lactate-epsilon-caprolactone (PLC) and polyglycolic acid (PGA) for the repair of a tendon bone junction. It was found that the use of a

polyglycolic acid (PGA) sheet promoted faster regeneration than the other two polymers with the formation of a well arranged fibrocartilage layer at the tendon bone insertion site. This was not observed when the polytetrafluoroethylene or the poly-L-lactate-epsilon-caprolactone scaffold was used. The PTFE sheet caused a chronic foreign body inflammatory response with minimal penetration of cells through the thickness of the PTFE, whereas the PGA sheet hydrolyzed rapidly and produced oriented fibrous tissue with a less intense inflammatory response. The PLC scaffolds had few chondrocytes attached to them, and those that were present were not aligned along the axis. In view of the fact that PLC degrades very slowly, it is not considered a suitable scaffold material for tendon bone junction regeneration. One of the major disadvantages of using a PGA sheet is that its mechanical properties are marginally inferior to those of natural tendons but it has significant potential for the regeneration of a tendon bone junction.

Hong Wei et al., [44] developed a knitted poly-lactide-co-glycolide (PLGA) scaffold to repair the defect in an injured Achilles tendon. Bone marrow stromal cells (bMSCs) were seeded onto the scaffolds which were implanted in the rabbits. Following the sacrifice, histological, immunohistochemical and biomechanical tests were carried out, and the results indicated that the knitted scaffold seeded with bone marrow stromal cells improved tissue regeneration and the repair of the defect in the injured Achilles tendon. The tissue formed by this scaffold was composed mainly of Type I and Type II collagen fibers and their strength was similar to that of natural tendon tissue.

2.4.Poly(lactic) Acid (PLA)

Poly(lactic) acid (Figure 2.10.a) is a thermoplastic aliphatic polyester derived from an α-hydroxy acid monomers. It is obtained from renewable resources such as starch and sugar. The building block of PLA is lactic acid (2-hydroxy propionic acid), which is a simple chiral molecule that can exist in two enantiomeric forms or stereo isomers, namely L- and D-lactic acid. Figure 2.10.b shows the structure of these two isomers of lactic acid.

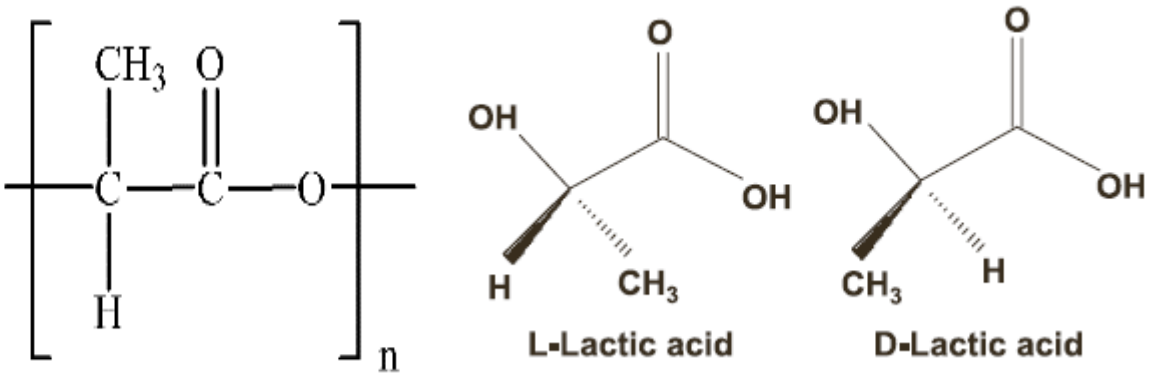

Figure 2.10 (a) Structure of poly(lactic) acid. (b)Enantiomers of lactic acid [38, 39]

Lactic acid is commonly produced commercially by fermentation of molasses, potato starch or corn. An alternative technique is to produce it from petrochemical feedstocks. The petrochemical method is shown in the Figure 2.11 and the lactic acid obtained by this method is a mixture of the L and D isomers which results in an optically inactive structure. On the other hand the lactic acid produced from corn starch by the bacterial fermentation method is primarily the L isomer with a small fraction (about 2%) of the D isomer.

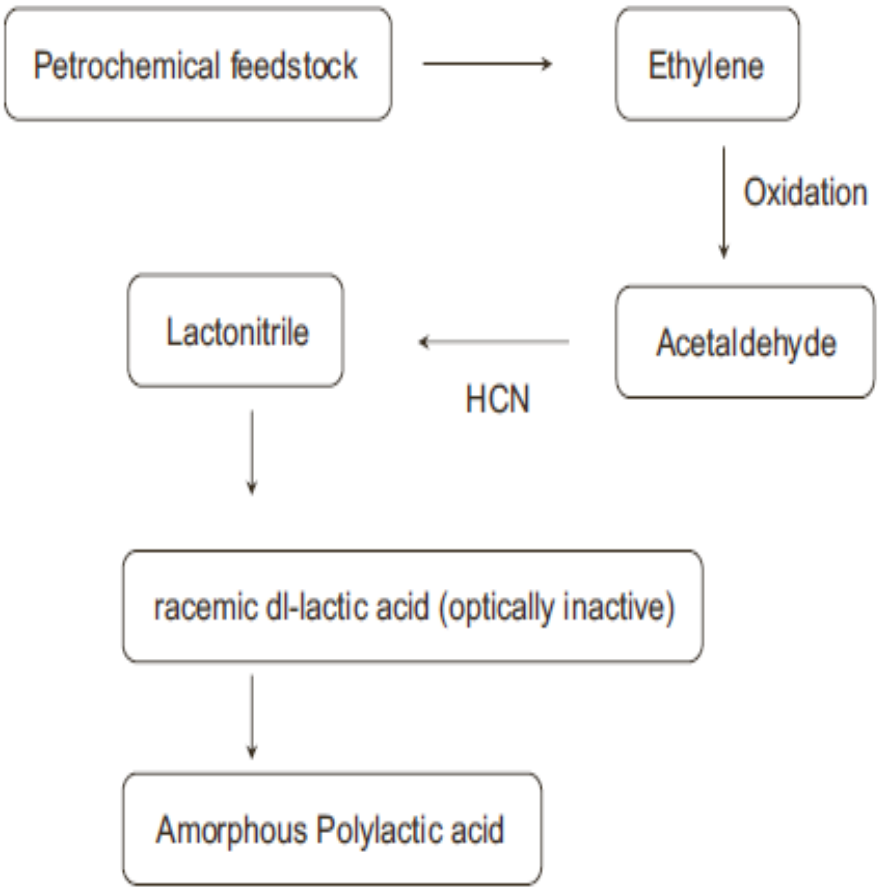

Figure 2.11 Petrochemical route for the production of lactic acid [38, 39]

The general life cycle of poly(lactic) acid (PLA) is shown in the Figure 2.12 It involves three basic steps. First PLA oligomers are formed by the removal of water from lactic acid, followed by the formation of lactide by depolymerization. Finally PLA is formed by polymerization of the monomer under vacuum distillation.

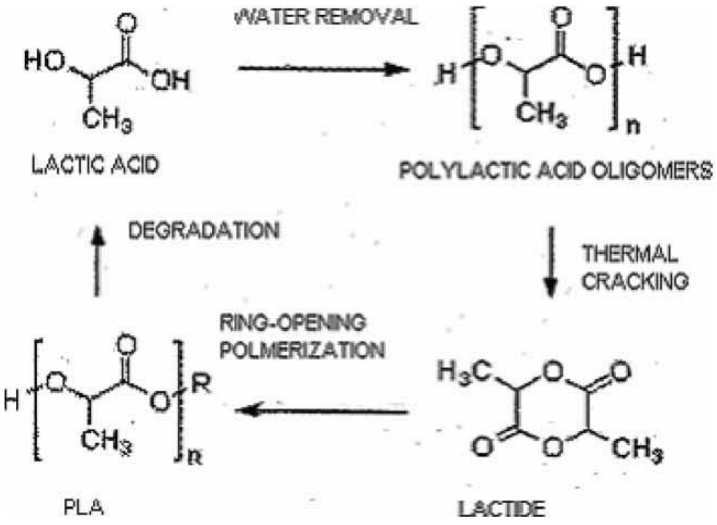

Figure 2.12 Lifecycle of poly(lactic) acid [40]

There are two ways in which lactic acid can be converted to poly(lactic) acid. The first method is the direct condensation method in which a solvent is used under high vacuum and temperature to remove the water produced by the condensation reaction. The disadvantage with this method is that the polymer produced has a low to intermediate molecular weight. The second method is a solvent free method where first lactide, a cyclic dimer, is formed and purified by distillation followed by catalytic ring-opening polymerization which produces poly(lactic) acid with a higher molecular weight [38, 41]. A flow chart of both the methods is shown in Figure 2.13.

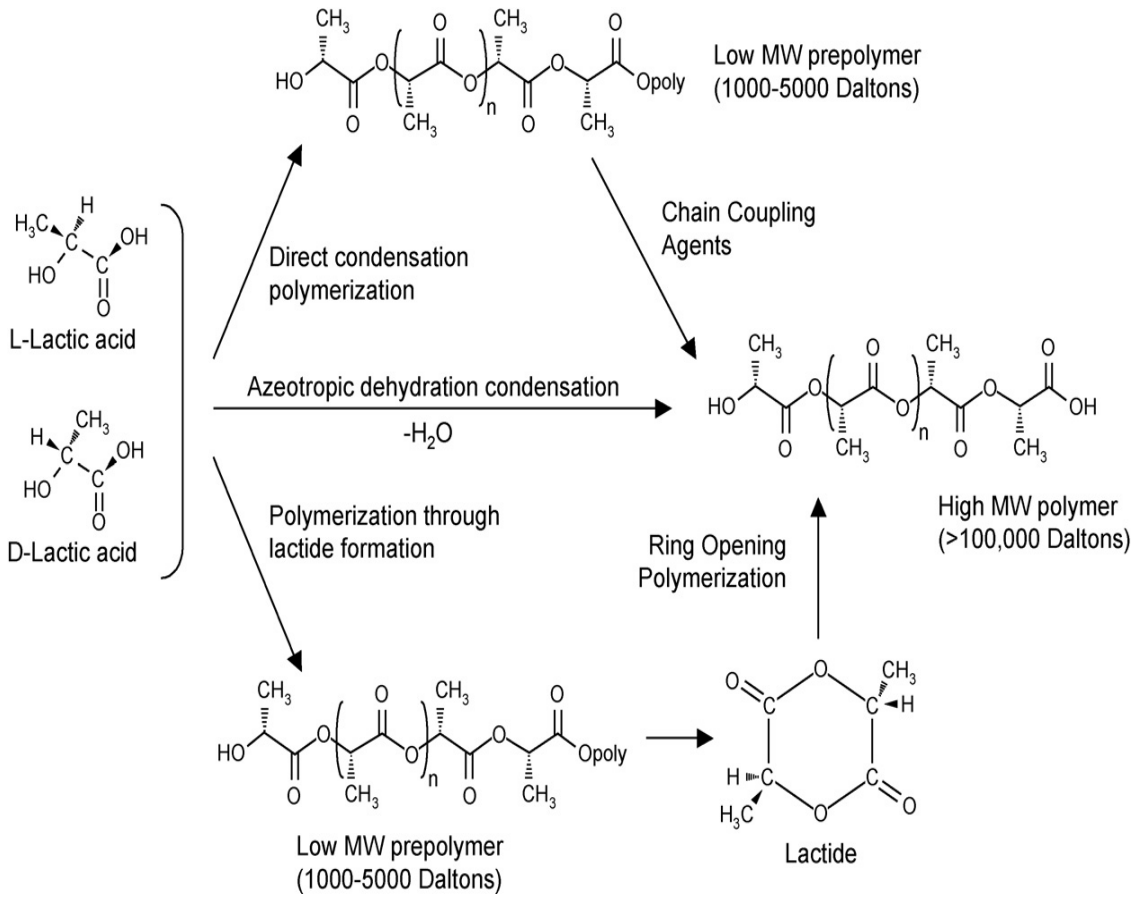

Figure 2.13 Synthesis of poly(lactic) acid [38,41]

The poly(lactic) acid polymer with a molecular weight in excess of 100,000 Daltons can be converted into fibers by extrusion of the polymer into mono or multifilament yarns either by a melt spinning, dry spinning, wet spinning or dry-jet-wet spinning approach [38]. Poly(lactic) acid fibers are thermoplastic, biocompatible and biodegradable. After drawing, they have high strength, high dimensional stability, high resiliency, low flammability and are UV resistant [39]. The properties of typical poly(lactic) acid fibers are listed in Table 2.3.

Initially when spun and drawn poly(lactic) acid fibers are hydrophobic in nature with a contact angle greater than 90 degrees. However, after exposure to a moist environment, PLA fibers can be used in applications where moisture transport is required. One such example of PLA is to melt spin fibers with four deep grooves (4DG). This unique cross-sectional shape can be fabricated to order by Fiber Innovation Technology Inc. (Johnson City, TN) which operates under a special license from Clemson University (SC). The spun and drawn fibers have multiple grooves as shown in Figure 2.14. Their cross-sectional shape was designed specifically to transport moisture along the length of each fiber. It also offers a greater surface area with the same high strength and uniform characteristics as expected from PLA fibers with a round cross-section[42, 43].

Figure 2.14 Morphology of 4DG fiber [43]

Table 2.3 Properties of poly(lactic) acid fibers [42]

Properties	Range of typical values
Density (g/cm^3)	1.210-1.430
Glass transition point (Tg)	40-70℃
Melting point (Tm)	130-180℃
Tensile strength (cN/tex)	4.0-4.8
Elongation at break(%)	30-40
Crystallinity (%)	Over 70
Young's modulus (kg/mm^2)	400-600

PLA has the potential to be used in wide range of applications in various field such as healthcare, medicine, apparel, sportswear, furnishing, filtration, packaging and composites. In the medical device industry it is used for making sutures, for surgical implants such as hernia repair meshes, for tissue engineering scaffolds as well as bandages and wound dressings. Since the primary degradation product of PLA is lactic acid, which is biocompatible and a normal product of healthy muscle function, PLA is widely used in a wide range of medical applications. The United States Food and Drug Administration (FDA) has approved the use of PLA as a polymer material for human clinical use in a number of implantable end uses [42].

Chapter 3

Materials and Methods

3.1 Fabrication of Scaffolds for Tendon Bone Junction Regeneration

This study involves the fabrication and evaluation of three different kinds of scaffolds for tendon bone tissue junction regeneration. The different fabrication and testing methods that were used are described in this chapter. The scaffolds were made from poly(lactic acid) fibers, a thermoplastic aliphatic polyester derived from renewable resources. Two types of PLA fibers were used to prepare the scaffolds. Round fibers with a diameter of 25 μm and 4DG fibers with a thickness dimension of 45 μm were used to prepare three different scaffolds. The three different scaffolds are 1) PLA hollow tubes using round fibers 2) PLA hollow tubes using grooved and round fibers (grooved fibers promote cell attachment and alignment) and 3) PLA bilayer tubes with round fibers and grooved fibers inserted inside the central hollow lumen (mimicking the bone region).

3.1.1 Preparation of PLA Yarns for Braiding

A novel grooved (4DG) fiber and a traditional round fiber made from poly(lactic acid) (PLA) melt spun by Fiber Innovation Technology Inc (Johnson City, TN) were used in this study. The PLA polymer containing 98% L isomer and 2% D isomer was supplied by Nature Works LLC (Minnetonka, MN, USA). The yarn with the round fiber had 72 nominal denier per ply and the yarn with the 4DG fiber had 60 nominal denier per ply. Both the yarns were multifilament yarns with 18 filaments per ply. The basic properties of both fibers are listed in Table 3.1. The grooved 4DG fiber is a fiber with four deep grooves along the fiber whose surface area is three times larger than the traditional round fiber. Figure 3.1 shows the cross

section shape of the traditional round and 4 DG fibers, after they have been compressed and cut during the sectioning preparation procedure. This explains why the observed fiber's cross-sectional appearance is distorted in Figure 3.1.

Table 3.1 Basic properties of the fiber

Type of fiber	Fineness (den/filament)	Cross sectional shape	Surface area (circumference of cross section)	Major channel area (width*length)
PLA 4DG	3	Grooved	375 µm	18.75 µm * 26 µm
PLA round	4	Round	112.5 µm	NA

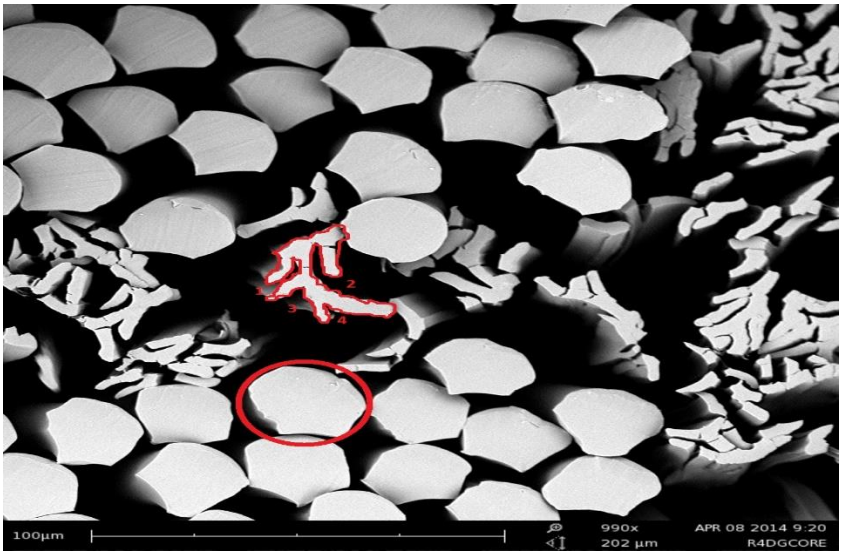

Figure 3.1 SEM image showing the cross sectional shape of the 4DG fibers and round fibers, after they have been compressed and cut during the sectioning preparation procedure

In order to mimic bone tissue, Scaffold No. 3 contains an additional core component that was inserted into the central lumen. The core component was a plied yarn. Since we were braiding a tubular scaffold with diameter of 1 – 1.5mm, we decided to insert a 10 ply 60d/18f 4DG yarn so as to achieve the desired yarn density and porosity. To prepare a 10-ply core yarn, ten 4 DG 60d/18f poly(l-lactic acid) (PLA) multifilament yarns were twisted together on a Direct-twist-2A twister (Agteks, Ltd) at 150 rpm. This plied yarn served as the core yarn to braid Scaffold No. 3 which consist of PLA bilayer tubes braided from round fibers with a 10 ply grooved fiber central core insertion. Since the single 4DG yarns had insufficient strength to withstand the tension during the braiding process, all the 4DG yarns used to braid the walls of the scaffold were 3 ply yarns. The 3 ply yarns were prepared by the same machine that was used to ply the 10-ply core 4DG yarns. The yarn that was produced by Fiber Innovation Technology Inc (Johnson City, TN, USA) was an undrawn round 170d/18f poly(l-lactic acid) (PLA) partially oriented yarn (POY) which was converted into a fully drawn 117d/18f PLA yarn (FOY) by using Model SW3 Drawing Tower (Hills Inc, Melbourne, FL) at the College of Textiles (Figure 3.2). Drawing was a two-step process at 76℃ with a wind up speed of 380 m/min. The draw ratio was 1.9 to 1. The basic properties of the fully drawn round PLA yarns that were used to braid the scaffolds are shown in Table 3.2

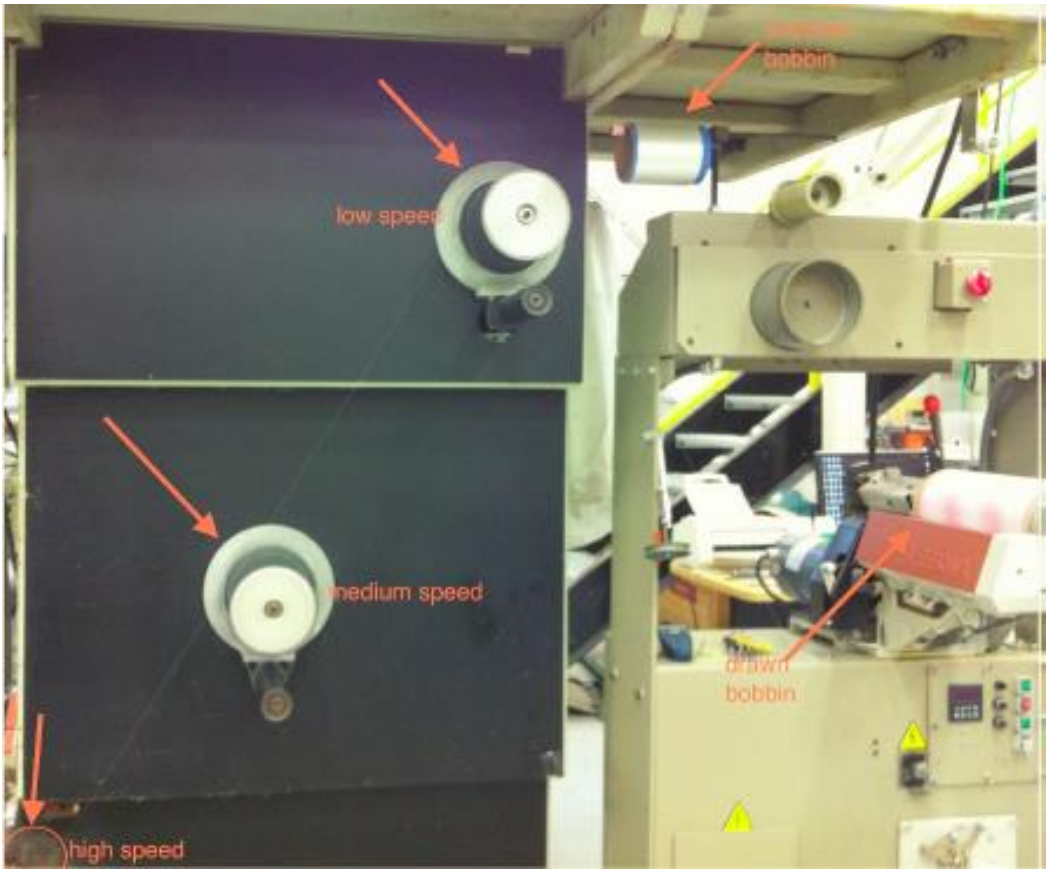

Figure 3.2 Drawing machine that was used to draw the round PLA yarns

Table 3.2 Properties of fully drawn round PLA yarn

Drawn 117/18 PLA	Cross-section	Crystallinity (%)	Tg (℃)	Tm (℃)	Density (g/cm^3)	Max Load (lbf)	Elongation at break (%)
	Round	31	60-65	173-178	1.24	0.721	23.34

3.1.2 Braiding of PLA Yarns

All three types of scaffold were braided on a Steeger USA 16-spindle braiding machine (Model K80/16-2008-SE), as shown in the Figure 3.3. In order to prepare Scaffold No. 1 (the PLA hollow tube with round fibers) the FOY 117/18 poly(l-lactic acid) yarn with round fibers was wound onto 16 small bobbins by the winding machine (Model: MS-888-SER.No. 60) to provide the supply packages for the Steeger braiding machine. The time taken by the winding machine to wind 500 yards was 3 minutes. The supply packages were mounted on the Steeger braiding machine and the PLA round hollow tubes were braided at 24 picks per inch and a braiding speed of 150 rpm.

Scaffold No. 2 (the PLA hollow tube with grooved and round fibers) was prepared in a similar manner except that 8 bobbins of FOY round PLA yarn and 8 bobbins of 3-ply 4DG PLA yarn were used instead of the previous 16 bobbins of FOY round PLA yarn.

Scaffold No. 3 (the PLA bilayer tubes with round fibers plus the central core of 10 ply grooved fibers) was prepared by a different method compared to the other two scaffolds. Single 4DG yarn was wound onto 10 small bobbins and inserted all together into the braiding machine through the central lumen so as to provide an additional core structure. The FOY round fiber PLA yarns were then braided around this central core of 10-ply 4DG PLA yarns. It was braided at 24 picks per inch with a braiding speed of 150 rpm.

Figure 3.3 Steeger braiding machine that was used to braid the scaffolds

A total of three different types of scaffolds were made to mimic the tendon bone tissue junction. They were:

1. PLA hollow tube using round fibers (RNC),
2. PLA hollow tube using both grooved and round fibers (the grooved fibers promote cell attachment and alignment) (4DGRNC) and
3. PLA bilayer tubes braided from round fiber yarns with an additional core component containing grooved fiber yarns (mimicking the bone region) (4DGRC).

After braiding the three scaffolds, the PLA tubular samples were thoroughly washed with 0.5% Triton-X solution (Sigma, T8787) at room temperature for 4 hours to remove any oils and other contamination that were deposited on the PLA scaffolds during braiding. Then they were rinsed with deionized water three times. The PLA scaffolds were then air dried inside a chemical hood at room temperature overnight. In order to prevent the PLA scaffolds from unraveling or distorting, the braided structures were heat set at 60℃ for 2 minutes in a Benz hot air oven.

3.1.3 Morphology by Scanning Electron Microscopy (SEM)

The surface morphology and cross-sectional view of the three different types of scaffolds were observed using a Phenom G1 scanning electron microscope (Phenom, Netherlands) after sputter coating the sample with gold-palladium in a SC7620 mini sputter coater (Quorum Technologies Inc, Canada). Images of the surface and cross-sectional views of the scaffolds were captured at magnifications in the x400 to x1000 range.

3.1.4 Total Porosity and Pore Size

Porosity is the measure of the total void content or empty spaces within a material. In a tissue engineered scaffold, the nature and extent of the porous structure will affect the cellular response and functionality. Total porosity can be determined by measuring the ratio of pore (void) volume to the total volume of a porous material and it is commonly expressed as a percentage [47].

The total porosity of the scaffolds can be calculated from the following equation:

$$\text{Total Porosity (\%)} = (1-d_S/d_{PLA}) \times 100$$

Where,

d_S = the density of the braided scaffold

d_{PLA} = the density of the PLA polymer

The density of the PLA polymer is 1.24 g/cm^3 [53]. The density of the braided PLA scaffolds was calculated from the mass of the scaffold and the cross sectional area of a 1cm long section of the braided scaffold. The cross-sectional area was calculated from the diameter of the scaffold which ranged between 1 and 1.5mm. The mass values were measured experimentally using a laboratory Mettler H80 balance (Switzerland).

Pore size and pore size distribution are different variables from total porosity. The pore size is a measurement of the dimensions of an individual pore or void space within a scaffold structure. There are various techniques to characterize the pore size such as adsorption, mercury intrusion, thermoporometry, x-ray scattering, electron microscopy, optical imaging etc. In this study scanning electron microscopy was used to determine the average individual pore size and the pore size distribution of the three braided scaffolds since the size of the pores lay in the range of 0.01 µm – 10 µm. A minimum of 10 specimens were visualized and measured using Image J software and the average values were calculated.

3.2 Mechanical Properties

3.2.1 Tensile Strength and Elongation at Break

The ultimate tensile strength of the three types of scaffolds were measured in the axial direction using an Instron mechanical tester, Model 2712-864 with a maximum load cell capacity of 2 kN. Bluehill 2 material testing software was used to record and analyze the results obtained from the mechanical tester. ASTM D5035-11 Standard Test Method for Breaking Force and Elongation of Textile Fabrics was the standard tensile strength test method that was followed. The test specimens were cut to a length of 40 mm so that they were long enough to be clamped in the top and bottom jaws of the mechanical tester and provide a gauge length of 10 mm. Five specimens were tested for each sample after the specimens were mounted, the cross head moved at a constant speed of 12 mm/min until specimen failure. The maximum load, elongation at maximum load and elongation at break were recorded. The maximum tensile strength and Young's modulus values were calculated from these values. The stress-strain curve was also obtained. Young's modulus E, was determined from the initial linear portion on the slope of the stress/strain curve.

The equation that was used to determine the Young's modulus is as follows

$$E=\frac{Tensile\ stress}{Tensile\ strain}=\frac{\sigma}{\varepsilon}=\frac{F/A}{\Delta L/L}=\frac{F\times L}{A\times \Delta L}$$

Where,

E = Young's modulus (MPa)

F = Absolute force applied to the fabric (N)

A = Original cross-sectional area of the scaffold (mm^2)

ΔL = Extension of the scaffold in axial direction (mm)

L = Original gauge length (mm).

The image of the Instron mechanical tester is shown in the Figure 3.4

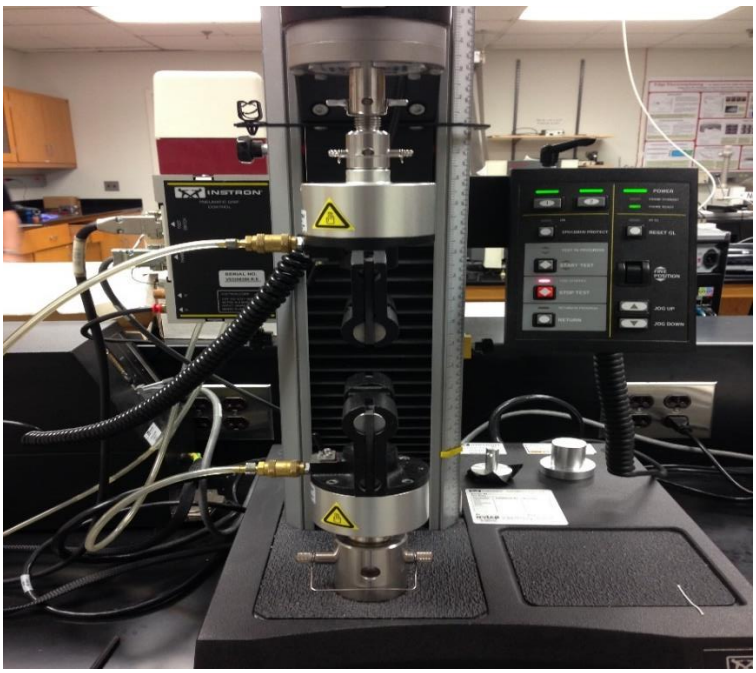

Figure 3.4 Instron mechanical tester that was used to test the mechanical properties of the scaffolds

3.3 In Vitro Cell Culture Study

3.3.1 Sample Preparation

Three types of scaffolds were involved in this study; namely, a PLA hollow tube using round fibers**,** a PLA hollow tube using grooved and round fibers (grooved fibers are believed to promote cell attachment and alignment) and a concentric PLA bilayer tube with round fibers and grooved fibers inserted inside the central hollow lumen (mimicking the bone region).All

three types of braided scaffolds were cut into 5 mm lengths and placed in a 96 well plate with one scaffold in each well.

3.3.1.1 Sterilization of the Scaffolds

The scaffolds were sterilized using ethylene oxide gas in an Auprolene Model AN74ix sterilizer (Anderson Products, Inc.) for 12 hours at ambient temperature. Following sterilization, the PLA braided scaffolds were aerated in a chemical hood for 48 hours so as to release any remaining ethylene oxide. The scaffolds were later immersed in 70% ethanol for 15 minutes followed by three rinses in 0.01 M phosphate buffered saline (PBS) (Sigma, P5244) (0.01M). In order to coat the scaffold with serum, the scaffolds were immersed in 10% fetal bovine serum (FBS) (Sigma, F1435) and kept overnight in an incubator at 37℃ and 5% CO_2.

3.3.2 TGF-β Type II Receptor Expressing Cells Isolation and Seeding

The Tgfbr2-β-Gal-GFP-BAC transgenic mice were allowed to mate and TGF-β Type II receptor expressing cells were isolated from 13.5/14.5 day old embryos of tenogenic Tgfbr2-β-Gal-GFP-BAC pregnant mice. The interval between E13.5 and E14.5 is critical in joint development because at E13.5 the interzone develops and by E14.5 the joint segments form from the adjacent growth plates. The embryos were removed and separated from the pregnant female mice [44]. The embryos were placed in an ice cold HBSS (Hank's Balanced Salt Solution, Sigma H6648). The whole autopod elbows and knees were removed by viewing the embryos under a dissecting microscope. The tissues were cut into small pieces and pooled in Dispase (1 µ/ml) for 45 minutes to 60 minutes at 37℃ with shaking of approximately 70 rpm. Dispase was prepared by dissolving the lyophilized powder in PBS (Phosphate Buffered

Saline, Sigma P5244) to give a 10 mg/ml solution, which was diluted to 2 µg/ml and filtered through a 0.22µm filter. The cells were filtered through a pre-wetted 40 µm cell strainer to remove any clumps and it was spun for 5 minutes at 1500 rpm. The PBS was removed carefully from the cell suspension and resuspend with about 1ml micromass medium which consisted of 40% DMEM-HG (Dulbecco's Modified Eagle's Medium, Sigma D5671), 60% Ham-F12, 10% FBS (Fetal Bovine Serum, heat inactivated, Sigma F4135) and Penicillin-Streptomycin (Sigma, P0781). The cell suspension was filtered again through a pre-wetted 40 µm cell strainer, and the cells were counted to be sure that the cell number was more than 1.0 x 10^7. The cells were then diluted with the micromass medium and taken for sorting. Isolation of TGF-β Type II receptor expressing cells was performed by FACS sorting (MoFlo, Beckman Coulter, Fullerton, USA) of mesenchyme limb cells from Tgfbr2-GFP-β-GEO-BAC that contained GFP (Green Fluorescent Protein) as gene reporters for Tgfbr2.

After sorting, the GFP+ cells were collected and counted again. They were later spun down. PBS was removed and resuspend with Micromass medium to ensure that the cell number was greater than 1 x 10^7/ml. The presorted and sorted TGF-β Type II receptor expressing cells with a total of 1.0 x 10^5 in 10 µl micromass medium were injected into the center of each prepared PLA scaffold and they were kept in the incubator at 37℃ and 5% CO_2 for 1 hour. Then 1 ml of micromass medium was pipetted into each well and it was changed every other day. The plates were incubated at 37℃ and 5% CO_2. Three specimens were used for each sample together with a control with only cells (no specimen). The cell suspension that was left after seeding on the scaffold were tested for cell viability. It was mixed with 0.4% of

trypan blue solutions in PBS and incubated for 2 to 5 minutes. Later the cell viability was tested by viewing under a microscope. Non-viable cells are known to be stained dark blue.

The biological performance of the three types of scaffolds with cells cultured on them were evaluated by the alamarBlue™ assay, laser scanning confocal microscopy (LSCM) with a live/dead stain and quantitative real time PCR (polymerase chain reaction) at different time points. The optical microscope images of the culture plate were also taken at different time points to determine when confluence of the cells occurred.

3.3.3 AlamarBlue™ Assay

The alamarBlue™ assay was used to evaluate the cell viability and cell proliferation on the three different types of scaffold at three different time points, namely: Day 3, 7 and 14. Living cells maintain a reducing environment inside the cytosol and the alamarBlue™ reagent uses this reducing power of the cells to confirm the viability. The alamarBlue™ reagent consists of an active component resazurin, which is a non-toxic, cell permeable compound that is blue in color and virtually non-fluorescent. When this compound enters a living cell, it is reduced into resorufin, a red colored compound which is highly fluorescent. This is the mechanism that the alamarBlue™ assay uses to quantify the viability of cells [49]. The three different types of scaffolds were taken from the 96-well plate and transferred into new plates and the medium from the old plate was pipetted out for the alamarBlue™ assay. The alamarBlue™ assay was carried out on the cells that were present on the scaffolds as well as those that was leaked to the plate. The alamarBlue™ assay was also carried out in the same way that was described above on the presorted cells. The alamarBlue™ solution for the study was prepared by adding 5% alamarBlue™ cell viability reagent (Life Technologies) to

95% micromass medium (40% DMEM, 60% Ham F12, 10% FBS, Pen Strep). 100 µl of the prepared solution was pipetted into each well containing the scaffolds and into each well of the old plate from which the scaffolds were taken out. Later the well plates were covered with aluminium foil to eliminate the light and kept in an incubator at 37℃ and 5% CO_2 for 24 hours. At the end of the incubation period, 50 µl of the liquid from both the plates were transferred to a new plate (Figure 3.5) and the level of fluorescence at the excitation wavelength range of 540 nm – 570 nm was measured with a Synergy micro-plate reader.

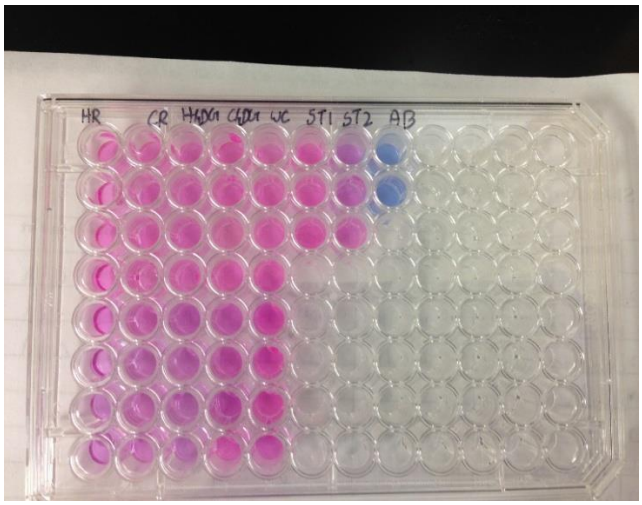

Figure 3.5 96 well plate with alamarBlue™ Assay indicating that the living cells have reduced the resazurin present in alamarBlue™ to resorufin leading to color change from blue to pink

3.3.4 Laser Scanning Confocal Microscope (LSCM) using Live/Dead Stain

The migration and attachment of cells along the surface and internal structure of the three different scaffolds was observed by a laser scanning confocal microscope (LSCM) after 3 and 7 days of culture. In order to visualize and differentiate the live cells from the dead cells, a live/dead cell double staining kit (Sigma – Aldrich) was used. The kit consisted of two

components, namely component A- Calcein-AM and component B-Ethidium homodimer-1 (EthD-1) solutions to stain live and dead cells respectively. Calcein AM is able to penetrate inside live cells, reacts with esterase and changes into calcein, which produces an intense green fluorescence, while Ethidium homodimer-1 enters dead cells and reacts with the damaged membrane to produce bright red fluorescence.

In order to prepare the samples for LSCM, a stock solution of 4µM EthD-1 was prepared by adding 20 µl of component B-Ethidium homodimer-1 to 10ml of sterile 1xDPBS (Dulbecco's Phosphate-Buffered Saline). Then 5 µl of component A-Calcein AM was added to 10 ml of the prepared stock solution 4µM EthD-1 to prepare the final experimental solution. The old medium was removed from the plates containing the three different types of scaffolds which were then washed three times with DPBS. Three small centrifuge tubes, one for each type of scaffold, was prepared with 3 ml experimental solution, and the three different types of scaffolds were transferred to the centrifuge tubes and incubated for 30-45 minutes at room temperature. Incubation was performed in a covered environment to prevent drying and contamination of the samples.

After incubation the samples were mounted on cover slips and observed under a Zeiss LSM 710 laser scanning confocal microscope (LSCM) (Carl Zeiss Micro imaging, USA). The scan head was attached to a Zeiss Axio Observer Z1 inverted microscope. Two dimensional images were obtained in a series of layers from the surface to the inner structure of the three types of scaffolds. The wavelengths used for imaging the live cells were λex~494 nm and λem~517nm, while the wavelengths used to view the dead cells were λex~528 nm and

λem~617 nm. Three-dimensional image reconstruction and analysis were performed using ZEN software (Carl Zeiss Micro imaging, USA).

3.3.5 Quantitative Polymerase Chain Reaction (qPCR)

Quantitative polymerase chain reaction is a powerful and sensitive gene analysis laboratory technique which is used for a wide range of applications such as quantitative gene expression analysis, genotyping, measuring RNA interference etc. It is also referred to as real time polymerase chain reaction given that it has the same components as the standard end-point PCR, but in addition it has a fluorescent label that can create a signal during the PCR reaction. The fluorescent label can be activated using either a non-specific fluorescent dye or a sequence-specific DNA probe. In this study qPCR was used to detect the gene expression of two important tendon proteins namely scleraxis and tenomodulin. The scleraxis protein is a member of the basic helix-loop-helix (bHLH) superfamily of transcription factors and early scleraxis expressing progenitor cells eventually lead to the formation of tendon tissue [54]. Tenomodulin is a member of the type II transmembrane proteins which play an important role in tendon development and vascularization [50].

In this study qPCR was performed on sorted TGF-β Type II receptor expressing cells and sorted TGF-β Type II receptor expressing cells cultured with the three types of braided PLA scaffolds for 3 weeks. Uncultured Sorted TGF-β Type II receptor expressing cells were included as the control. Sample preparation for qPCR involved two steps – extraction of mRNA and synthesis of cDNA. Here mRNA's from the TgfbR2 positive cells were extracted and reversed transcribed into cDNA by using µMACS mRNA isolation and synthesis kit (Milteyi Biotec). Those cDNA's were detected and quantified by qRT-PCR (MyiQ, Bio-Rad)

using SYBR green dye (Bio-Rad) which is a cyanine dye used in biology as a nucleic acid stain. It has the ability to intercalate with double-stranded DNA and this intercalation causes the fluorescence which is in turn detected by the qPCR. The values from the intensity of the fluorescence were obtained using the Gene Expression Analysis Software (Bio-Rad, Hercules, CA, USA). The expression of genes of interest were normalized using glyceraldehyde 3-phosphate dehydrogenase(GAPDH) expression because the GAPDH gene is stable and usually expressed at high levels in most cells. It is considered as the control or housekeeping gene [55].

3.4 Statistics

The mean and standard deviation were calculated for all the tests. Statistical comparisons were made between the test groups and the controls using a standard t-test. The alpha value was assumed to be 0.05. Values less than or equal to 0.05 were considered statistically significant.

Chapter 4

Results and Discussion

4.1 Characterization of the Braided Scaffolds

4.1.1 Structure of the Braided Scaffolds

Two types of PLA fibers, namely fibers with a 25μm diameter round cross-section, and grooved fibers with four deep grooves (4DG) and measuring 45μm in thickness, were used to prepare three different types of scaffold to mimic the tendon-bone tissue junction. The three types of scaffold were:

1) PLA hollow tubes using round fibers (RNC)

2) PLA hollow tubes using grooved and round fibers (4DGRNC) and

3) PLA bilayer tubes with round fibers and grooved fibers inserted inside the central hollow lumen (4DGRC).

The microstructural images of the three types of scaffolds were taken under scanning electron microscopy at different magnifications. Both the cross sections and the surfaces were imaged. Figure 4.1 shows the cross sectional view and the longitudinal surface view of the round hollow tube with no central core. It shows that the surface was smooth since it contained only yarns with the round PLA fibers. Figure 4.2 shows the cross sectional view and longitudinal surface view of the mixture of 4DG and round fibers braided into a hollow tube with no central core. Since it contained 4DG fibers in its structure, it had a larger surface area compared to Scaffold 1 with only round fibers, and the surface was not as smooth as observed with Scaffold 1.

Figure 4.3 shows the cross sectional view and longitudinal view of the PLA concentric bilayer tube with round fibers in the sheath and 4DG fibers inserted inside the central hollow lumen. The cross sectional view shows how the core 4DG fibers are surrounded by the round fibers. The surface morphology of all three types of braided structure illustrates a porous structure due to the interlocking of the braided yarns.

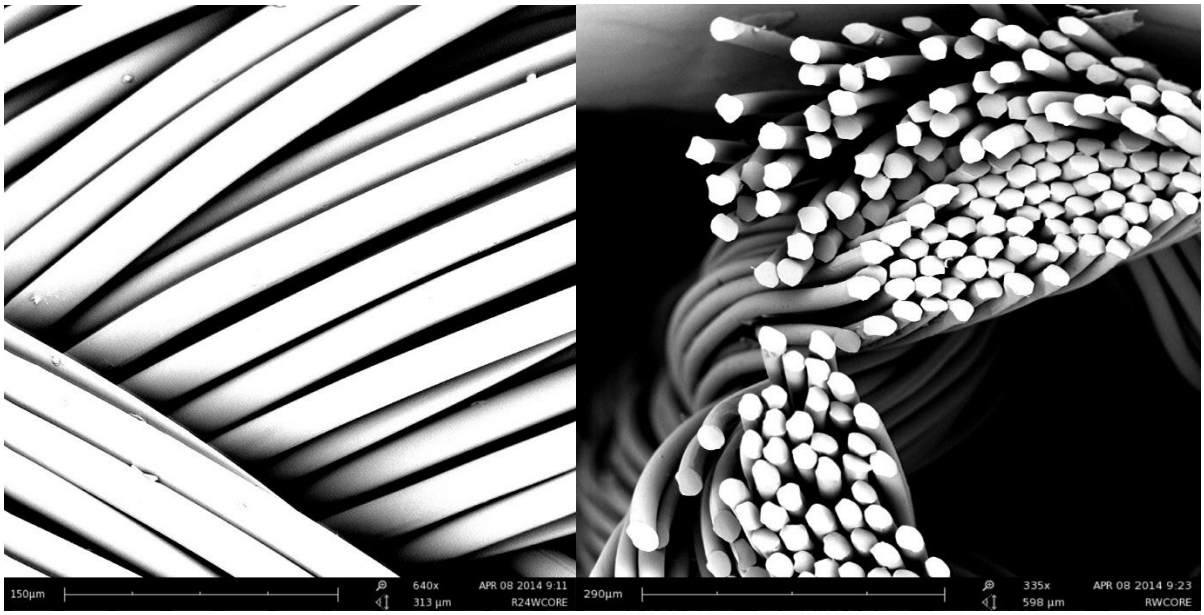

Figure 4.1 Cross sectional view and longitudinal surface view of the round hollow tube with no central core

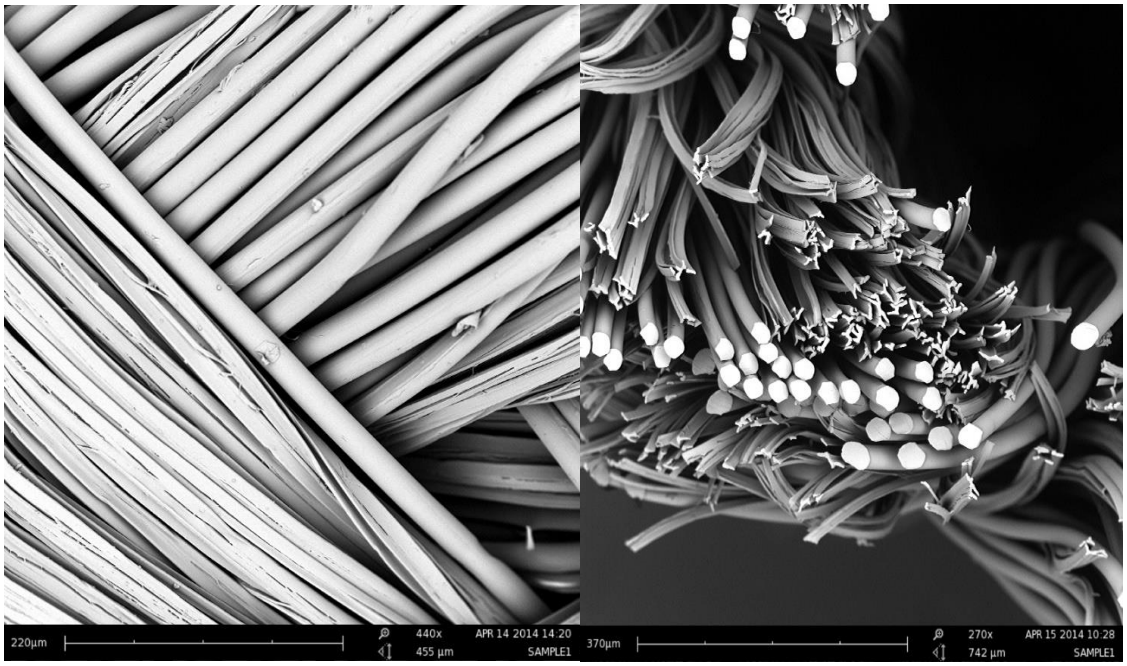

Figure 4.2 Cross sectional view and longitudinal surface view of the 4DG and round fibers forming an empty hollow tube with no core

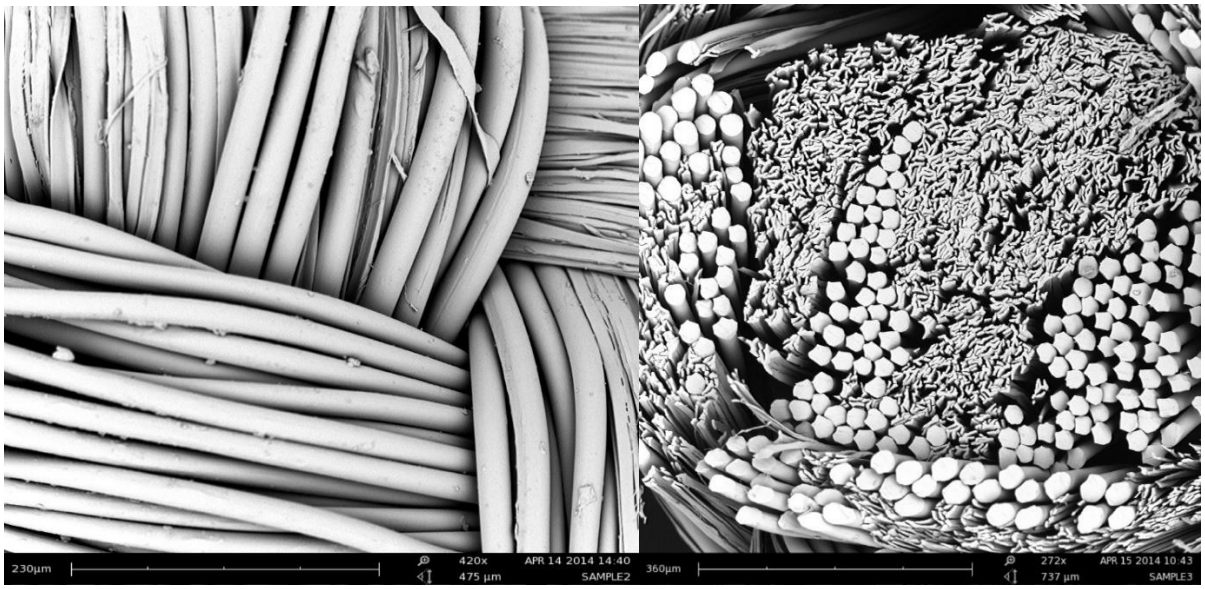

Figure 4.3 Cross sectional and longitudinal views of the PLA concentric bilayer tube with round fibers in the sheath and 4DG fibers inserted inside the central lumen

4.1.2 Basic Properties of the Braided Scaffolds

Braided structures have several advantages over other tubular structures. They can produce soft, flexible and semipermeable tubes that can be placed inside a living system without any complications. The braiding angle θ is calculated from the following equation [56].

$$\theta = \tan^{-1}\frac{2\pi(D+2d)P}{C}$$

Where D is the diameter of the braided tube (inch), d is the diameter of the yarn (inch). P is the pick count (picks/inch) and C is the number of carriers. The average diameter of the braided tubes was first determined using the compression resistance tester, but also by analyzing the images taken by SEM. For all three types of braids the diameter of the braid was found to be 1.2 mm. The average diameter of the round fibers was 25 μm and the average thickness of the 4DG fibers was 45 μm. The braided pick count was 24 picks/ inch for all three types of braid. The number of carriers was 16 since the Steeger braiding machine had 16 spindles. By using these measurements in the braiding angle equation, the braiding angle was calculated to be 26°. The braiding angle measured from SEM images was in agreement with this calculated value [Figure 4.4]. The average pore size for the braids where the yarns cross was close to zero. In addition there were some pores ranging from 5 to 25 μm between individual yarns [Figure 4.4]. These pores can help in the exchange of oxygen and providing nutrition. The total porosity for all three types of scaffold was calculated using the equation mentioned in Chapter 3. The basic properties of the three types of scaffolds braided for this study are summarized and listed in Table 4.1.

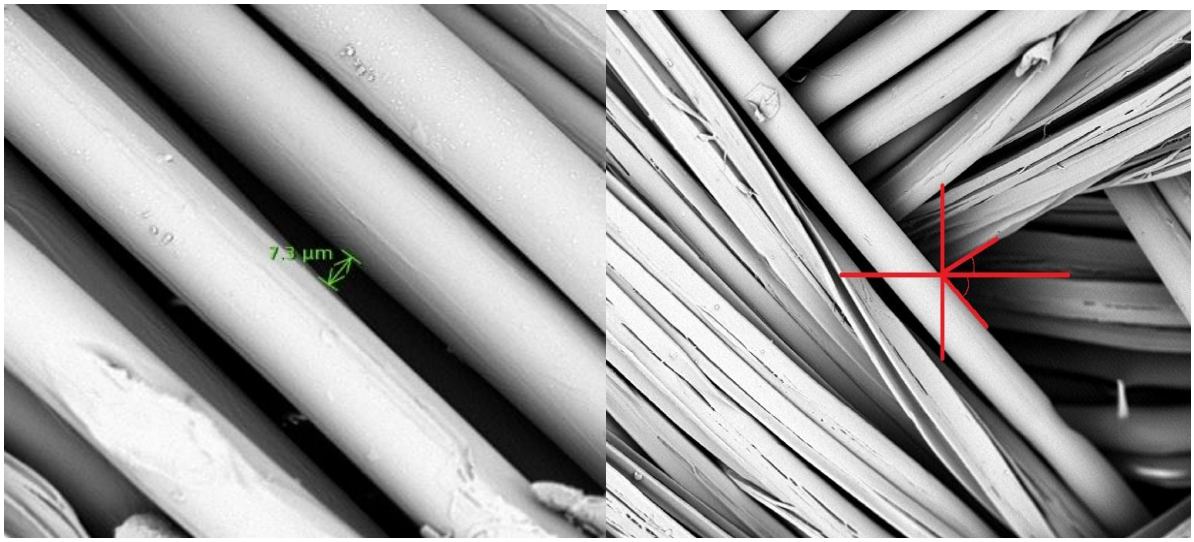

Figure 4.4 SEM images of the PLA braided scaffolds showing the pore size (left side) and braiding angle (right side)

Table 4.1 Basic properties of the three types of braided scaffolds

Types of Scaffold	Mass (mg)	Length (mm)	Diameter (mm)	Total Porosity (%)	Pore size range (µm)	Braiding angle (°)
RNC	7.8	20	1.2	72.17	5-25	26
4DGRNC	6.9	20	1.2	75.38	5-25	26
4DGRC	11.3	20	1.2	60.42	5-25	26

The ideal tissue engineered scaffold should have a total porosity in the range of 50% - 80% to support the culture of cells and the diffusion of nutrients throughout the whole structure of the scaffold [51]. The individual pore size should be in the range of 5-15 µm for fibroblast ingrowth and around 200 µm for osteo-conduction [51]. The total porosity of all three types

of developed scaffolds were within the required range confirming that the scaffolds were able to support cell ingrowth, uniform cell distribution and the transfer of oxygen and nutrients. The pore size of the scaffolds RNC and 4DGRNC mimicking the tendon was 5 – 25 μm, which has been reported to be ideal for certain cell ingrowth. But the average pore size of the 4DGC mimicking the bone could have been higher in order to facilitate osteo-conduction. However the scaffold mimicking the bone had 4DG fibers with deep grooves on their surface that increased the surface area of the scaffold, which in turn improved the penetration of cells and exchange of nutrients.

4.2 Mechanical Properties

The three types of scaffolds were fabricated to mimic the physical properties of a tendon to bone junction. It was therefore important to measure the mechanical properties of the scaffold structures and compare them with tendon and bone tissues. The ultimate tensile strength and Young's modulus of the three types of scaffolds were measured in the axial direction. Figure 4.5 shows the ultimate tensile strength for the three types of scaffolds. Standard deviation was used to generate the error bar and a standard two tailed t-test was carried out to compare the three different types of scaffolds. The ultimate tensile strength of the 4DGRC scaffold mimicking the bone was significantly higher than the ultimate tensile strength of the scaffolds mimicking the tendon, namely the two hollow scaffolds without the core. P values were 0.0059 and 0.018, which are less than the alpha value of 0.05. The ultimate tensile strength of the two hollow scaffolds mimicking the tendon were not significantly different from each other (p value = $0.07 \geq 0.05$). Hence the insertion of core in the braided structure increases the tensile strength significantly to mimic the hard bone tissue.

The mean elongation values of the three types of scaffolds are showed in Figure 4.6. Standard deviation was used to generate the error bar and a standard two tailed t-test was carried out to compare the elongation values for the three different types of scaffolds. There were significant differences between all three scaffolds ($p \leq 0.05$). The hollow scaffolds with round fibers had the maximum elongation followed by the hollow scaffold with 4DG and round fibers, and then the scaffold with braided round fibers and 4DG fibers in the inserted central core.

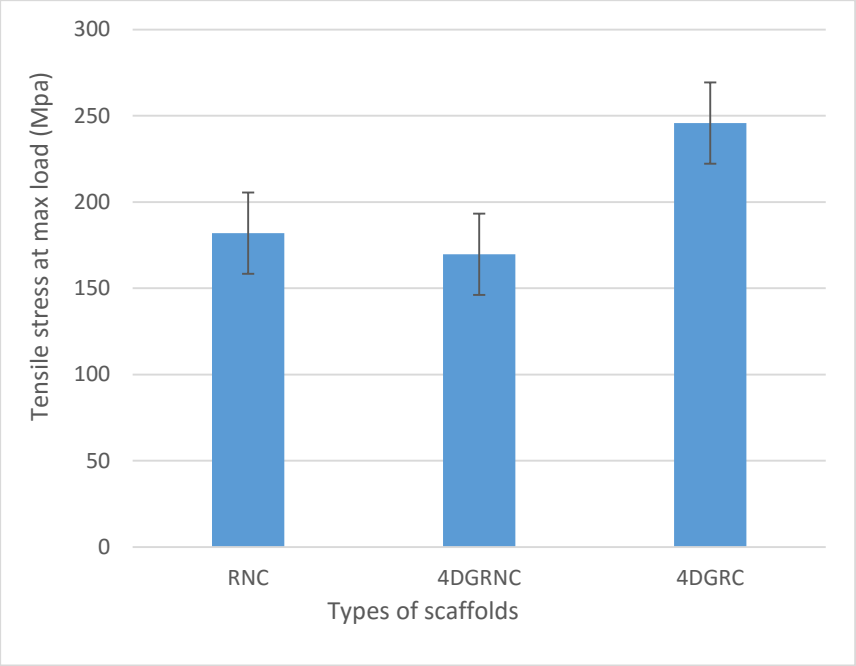

Figure 4.5 Ultimate tensile strength of the three types of scaffolds: 4DGRC was significantly higher than RNC & 4DGRNC

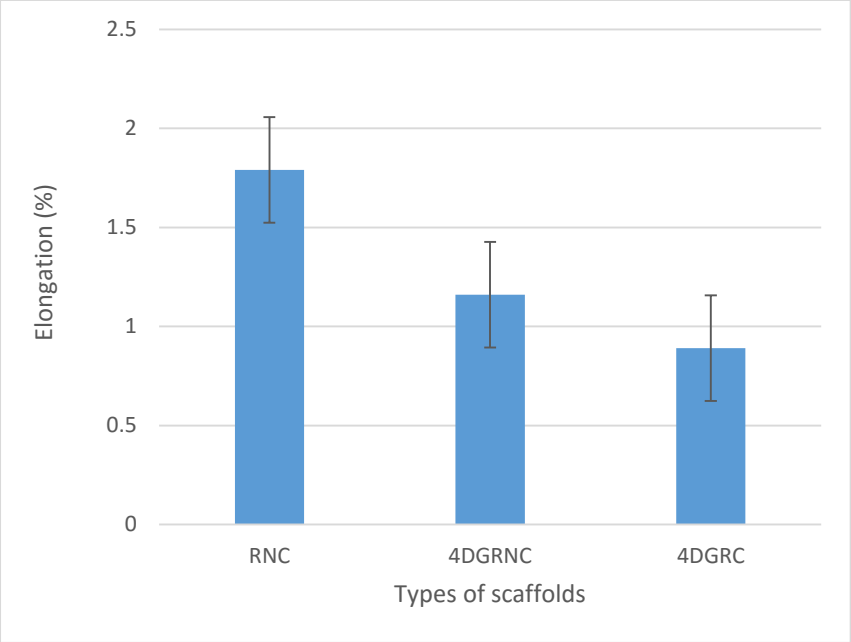

Figure 4.6 Elongation values of the three types of scaffolds: RNC had the highest value followed by 4DGRNC & 4DGRC

Figure 4.7 shows the Young's modulus values for all three types of scaffolds. The Young's modulus value of the bilayer tube with central core insertion was significantly higher than the other two hollow scaffolds without the additional central core ($p \leq 0.05$), whereas there was no significant difference between the Young's modulus values of the two hollow scaffolds without a central core ($p \geq 0.05$). The Young's modulus values for the scaffolds were compared with the Young's modulus values for a human tendon and bone tissue (Table 4.2). In particular, the Young's modulus values for the two hollow scaffolds mimicking the tendon were similar to that of a human tendon, and likewise the Young's modulus value of the bilayer braided scaffold with core insertion was in the same range as the Young's modulus value of human bone [52]. Thus the three different braided scaffold structures provide a wide

range of mechanical properties that mimic the component parts of a tendon bone tissue junction.

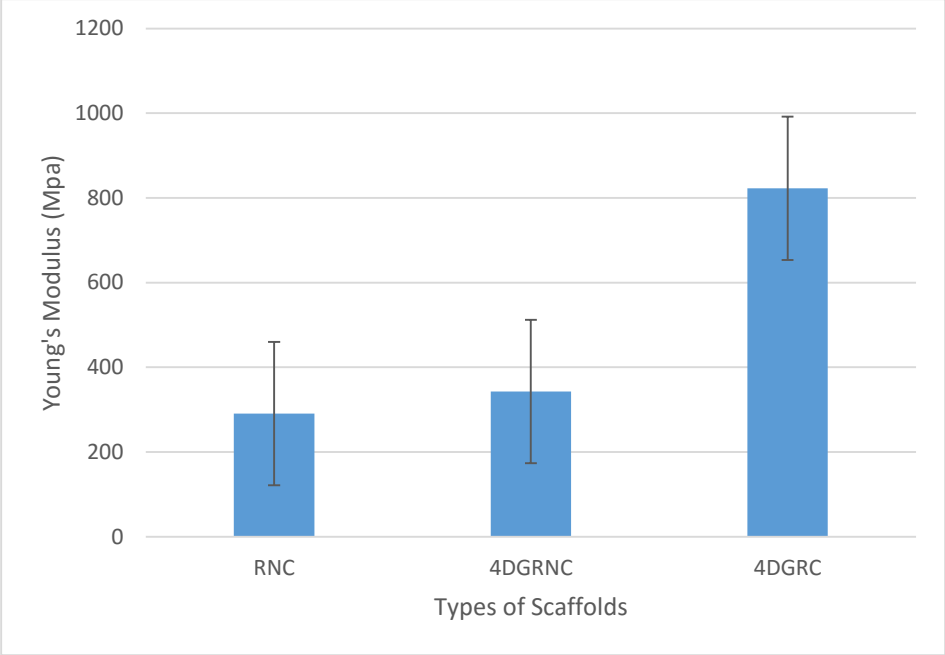

Figure 4.7 Young's modulus values of the three types of scaffolds: 4DGRC mimicking the bone had the highest value followed by RNC & 4DGRNC mimicking the tendon

Table 4.2 Mechanical properties of the three scaffolds and natural tissues

Young's Modulus (MPa)	PLA hollow tube with round fibers	PLA hollow tube with 4DG & round fibers	PLA bilayer sheath with 4DG core insertion	Human Tendon	Human Bone
	290	342	822	250	700 – 18,000

4.3 Biological Performance of the Scaffolds

4.3.1 Optical Microscopic Images of Cell Attachment

When the cells were seeded onto the scaffolds, some of the cells leaked out from the scaffold and attached themselves to the two dimensional bottom surface of the well plate. Figures 4.8, 4.9, 4.10 and 4.11 show the optical images of the well plates in which the cells had been seeded onto the scaffolds after 1, 3, 7 and 14 days of culture respectively. The images show that the cells grew next to the three types of braided scaffolds in the same well. They confirm that the braided scaffolds did not release any cytotoxic degradation by-products that might have been harmful to the cells. There was no significant difference in the morphology of the cells between the control group, having only cells and no scaffold, and the test groups with the braided scaffolds. There was little difference between the number of cells observed at Day 1 and Day 3, but the confluence of cells increased significantly by Day 7, and by Day 14 it was above 95%.

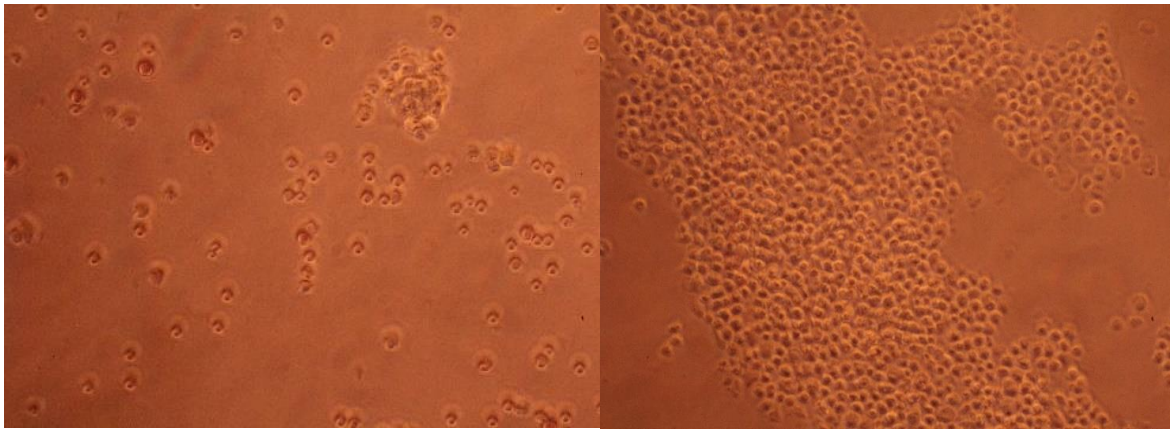

Figure 4.8 Optical microscopic images of well plates containing the scaffold (left) and the control with no scaffold (right) on Day 1

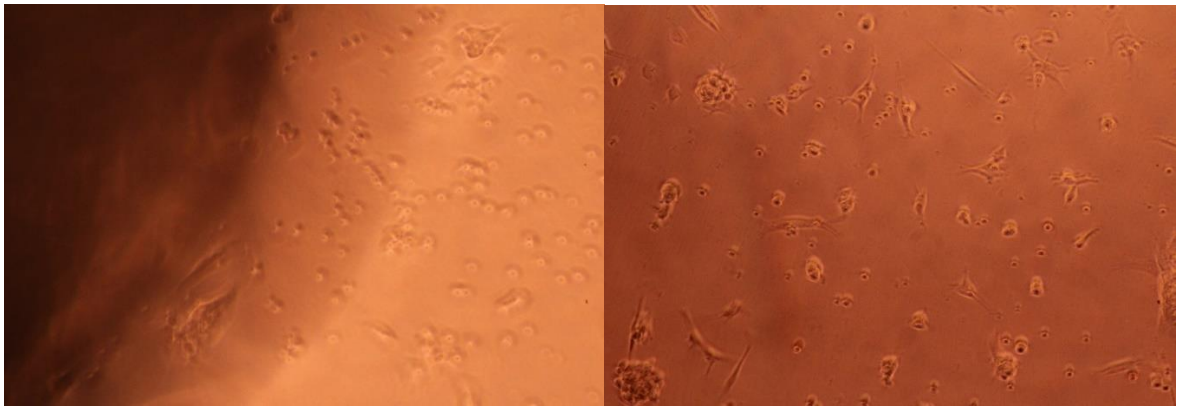

Figure 4.9 Optical microscopic images of well plates containing the scaffold (left) and the control with no scaffold (right) on Day 3

Figure 4.10 Optical microscopic images of well plates containing the scaffold (left) and the control with no scaffold (right) on Day 7

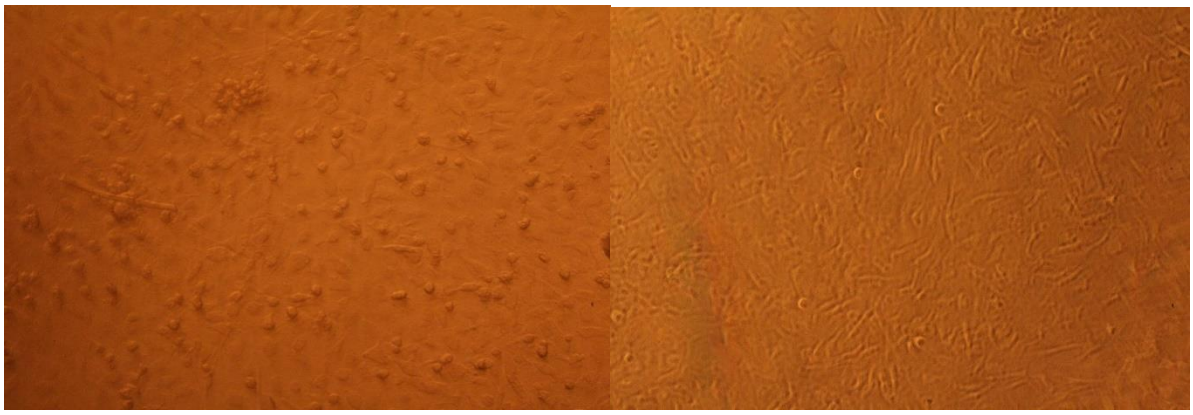

Figure 4.11 Optical microscopic images of well plates containing the scaffold (left) and the control with no scaffold (right) on Day 14

4.3.2 AlamarBlue™ Assay

The alamarBlue™ assay was used to evaluate the extent of cell viability and cell proliferation of the TGF-β RII cells on the three different types of scaffold. The fluorescence values of the cells cultured on the three different scaffolds were measured at Day 3, 7 and 14. Figure 4.12 shows the fluorescence values of the sorted TGF-β Type II receptor expressing cells at various time points, and similarly, Figure 4.13 shows the fluorescence values of the presorted TGF-β Type II receptor expressing cells at various time points. The cells that were cultured directly on the plate was considered as the control. On comparing the extent of cell proliferation at different time points for both the sorted and presorted TGF-β Type II receptor expressing cells, it can be seen that on Day 14 the cell proliferation was significantly higher than the cell proliferation on Day 3 ($p \leq 0.05$). This result shows that the cells were continuously proliferating and were not controlled by the presence of the scaffolds, indicating that all three types of scaffolds are biocompatible and not cytotoxic. By comparing the fluorescence values of the scaffolds and well plates, it can be concluded that there was

greater cell viability on the scaffolds compared to the plates. The well plates were uncoated whereas the scaffolds were coated with fetal bovine serum before seeding, which could have increased the proliferation and viability of the cells. The fluorescence values of the sorted TGF-β Type II receptor expressing cells were lower than that of the presorted TGF-β Type II receptor expressing cells. This was primarily due to the smaller seeding density of the sorted TGF-β Type II receptor expressing cells.

On comparing the three different types of scaffolds on Day 3, the hollow scaffold with round fibers showed a marginally higher viability and proliferation compared to the hollow scaffold with round and 4DG fibers and the bilayer scaffold with the central core of 4DG fibers. On Day 7 and Day 14 the two hollow scaffolds showed similar values. At the same time the 4DG fibers had a marginally faster proliferation rate due to the grooves present in the 4DG fibers, which resulted in an increase in surface area for the cells to attach to and proliferate.

On comparing the scaffold with a central core to the hollow scaffolds, the rate of cell proliferation on the hollow scaffolds with no core was marginally faster than for the scaffolds with a core. It is thought that this was due to the lower porosity of the hollow scaffolds. In summary, the hollow scaffolds coated with fetal bovine serum showed the highest cell viability and cell proliferation result among the three different braided scaffolds.

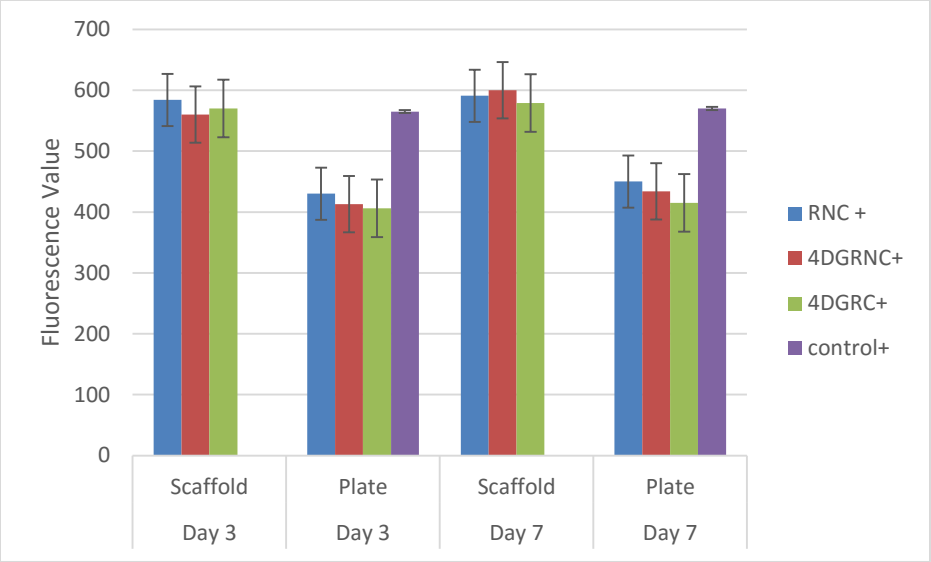

Figure 4.12 Fluorescence values of the sorted TGF-β Type II receptor expressing cells at various time points showing greater cell proliferation & viability on the scaffolds than on the plate

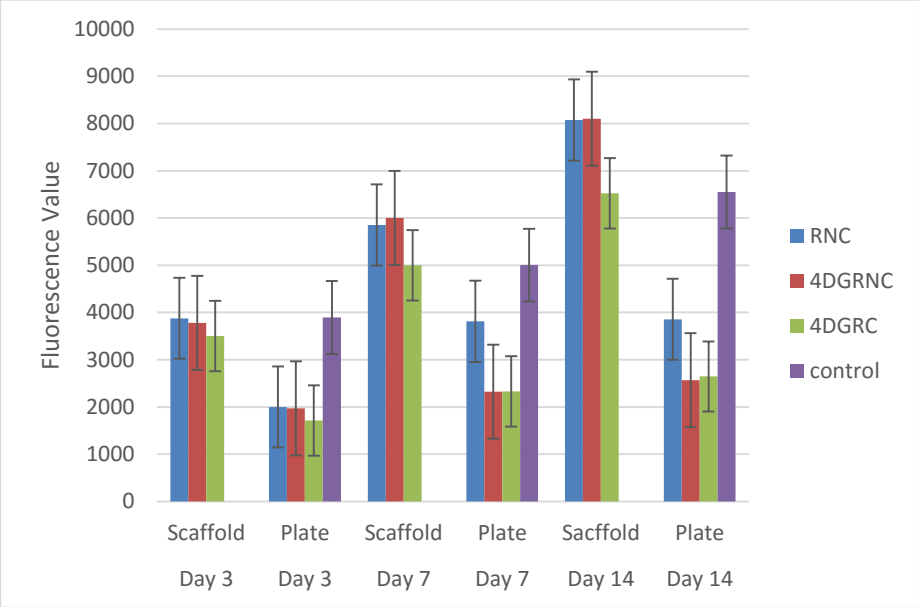

Figure 4.13 Fluorescence values of the presorted TGF-β Type II receptor expressing cells at various time points showing greater cell proliferation & viability on the scaffolds than on the plate

4.3.3 Laser Scanning Confocal Microscope (LSCM) using Live/Dead Stain

Laser scanning confocal microscopy was used to determine the extent of migration and attachment of cells on the three different types of scaffolds. In addition, the viability of the cells was also determined using the live and dead stain. The difference in wavelength of the two components in the staining kit enabled us to identify the live and dead cells. If the cells were alive, they appeared green under the confocal microscope and if the cells were dead they appeared red in color. The images of all three types of scaffolds with cells were taken on Day 3 and Day 14. Figures 4.14 and 4.15 shows the cell attachment on the three different braided scaffolds on Day 3 and Day 7 respectively at a lower magnification. The images indicate that the cells have penetrated inside the scaffolds and attached to the PLA fibers. They also show that the ratio of green live cells to red dead cells was greater than 1. In order to obtain a clearer view of the cellular performance, images containing only live cells and images with only dead cells were obtained separately using the ZEN software.

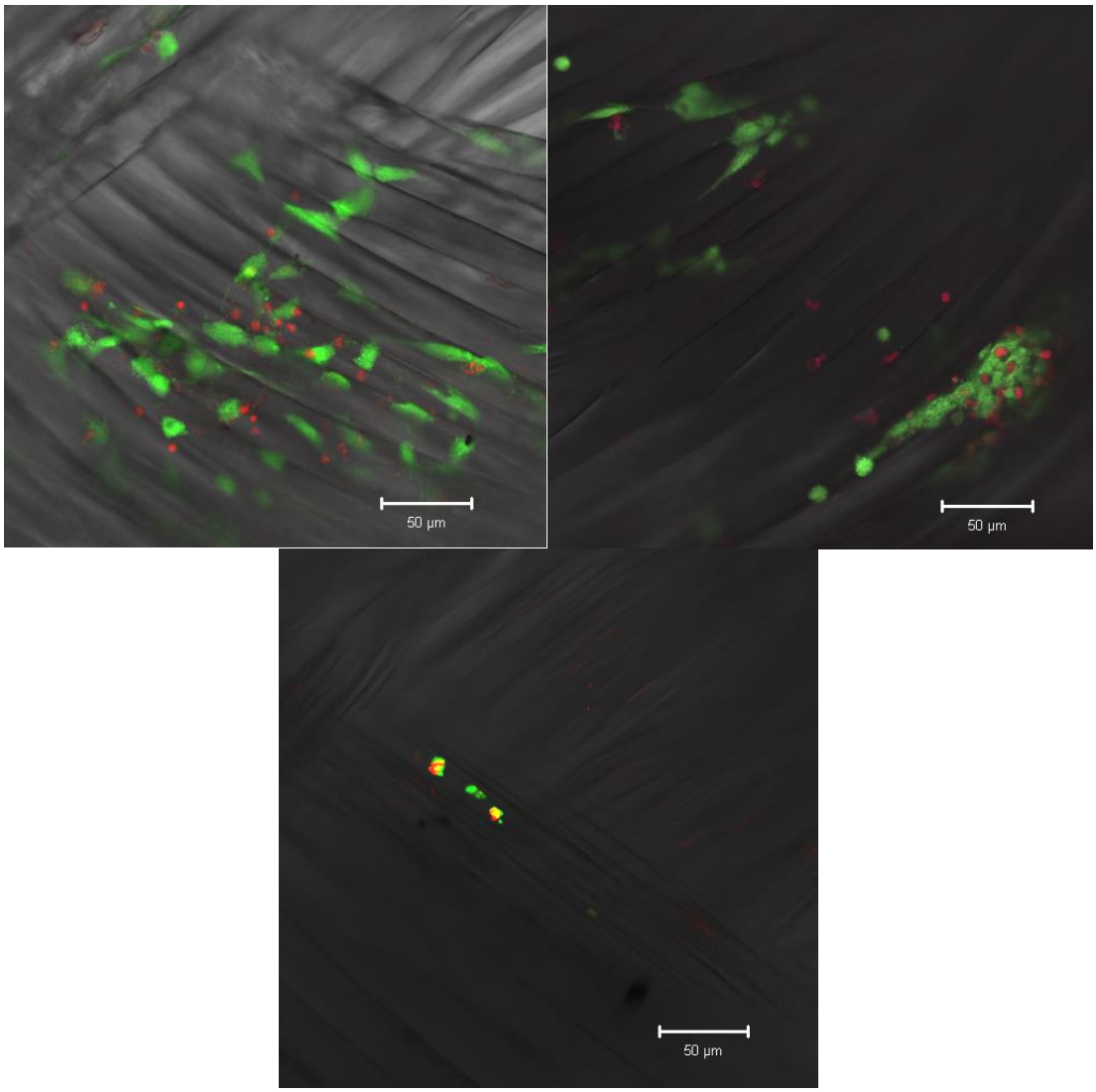

Figure 4.14 Cell attachment on the three different braided scaffolds on Day 3; RNC - top left, 4DGRNC – top right, 4DGRC – bottom; green indicates live cells and red indicates dead cells

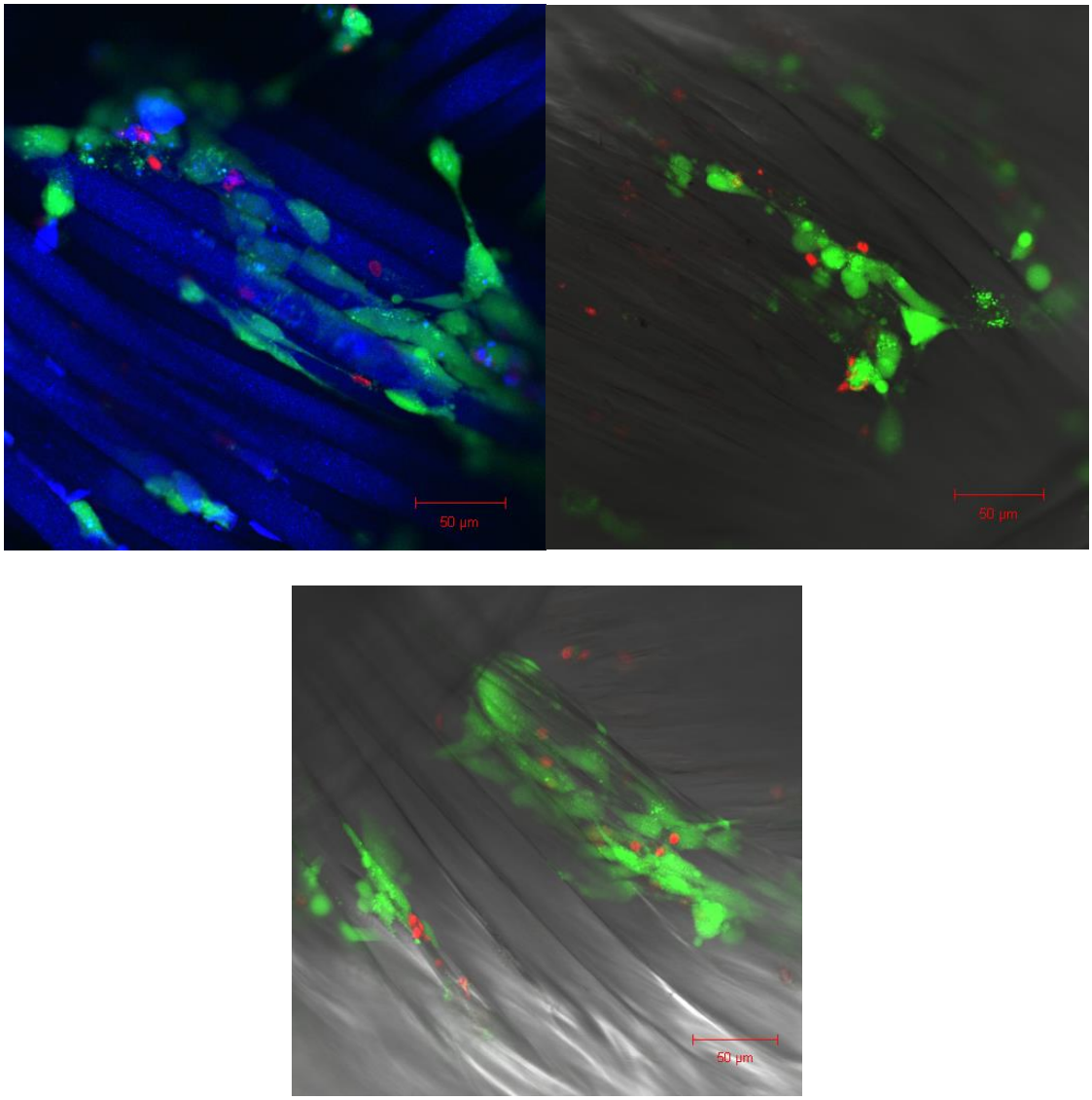

Figure 4.15 Cell attachment on the three different braided scaffolds on Day 7; RNC - top left, 4DGRNC – top right, 4DGRC – bottom; green indicates live cells and red indicates dead cells

Figures 4.16, 4.17 and 4.18 show the three dimensional images of live and dead cells at Day 3 on the hollow scaffold with round fibers, on the hollow scaffold with 4DG fibers and on the bilayer scaffold with 4DG fibers in the central core respectively. The cell viability on the hollow scaffold with round fibers was the highest, followed by the hollow scaffold with 4DG

fibers and then the bilayer scaffold with the central core. There were more green cells than red in the images, which indicates that the cells preferred to grow on the PLA fibers and that the cells spread throughout the scaffold indicating that cell migration was positive.

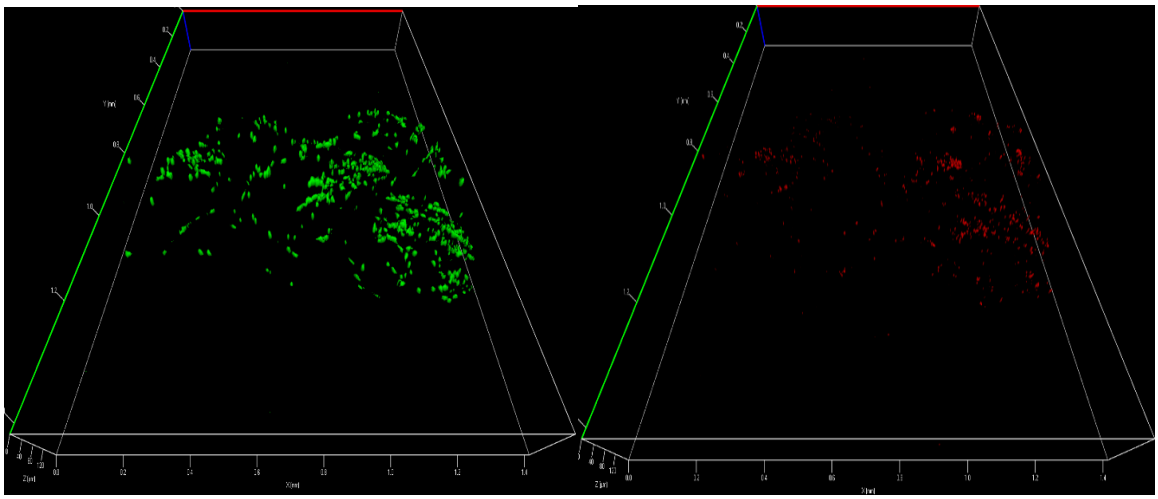

Figure 4.16 Three dimensional images of live (green) and dead (red) cells on the hollow scaffold with round fibers on Day 3

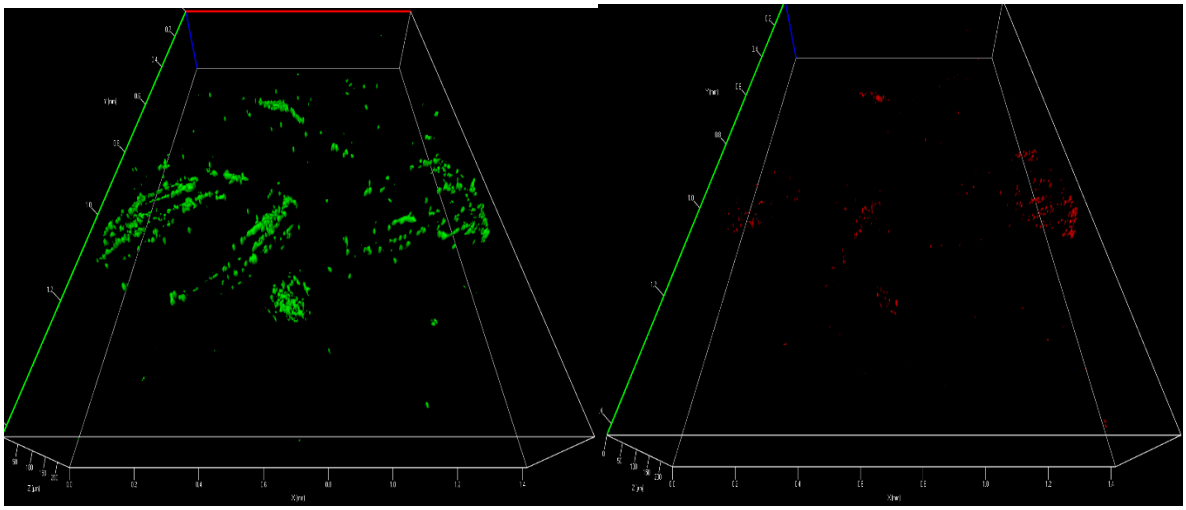

Figure 4.17 Three dimensional images of live (green) and dead (red) cells on the hollow scaffold with 4DG fibers on Day 3

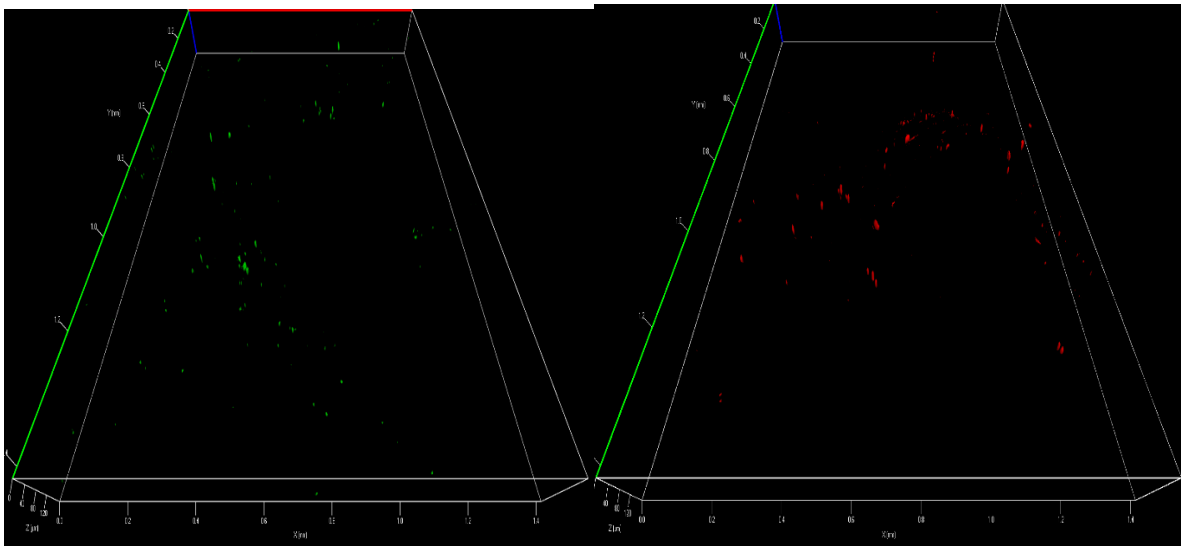

Figure 4.18 Three dimensional images of live (green) and dead (red) cells on the bilayer scaffold with 4DG fibers in the central core on Day 3

Figures 4.19, 4.20 and 4.21 show the three dimensional images of live and dead cells at Day 7 on the hollow scaffold with round fibers, on the hollow scaffold with 4DG fibers and on the bilayer scaffold with 4DG fibers in the central core respectively. Compared to Day 3, the images at Day 7 showed more green cells, confirming that cells were continuously proliferating and that the PLA fibers supported cell viability even after 7 days of culture. The cells were observed to be present throughout the thickness of the scaffold, which demonstrates that the PLA fibers were biocompatible, and that the experimentally designed structures of the braided scaffolds were able to promote cell viability, proliferation and migration.

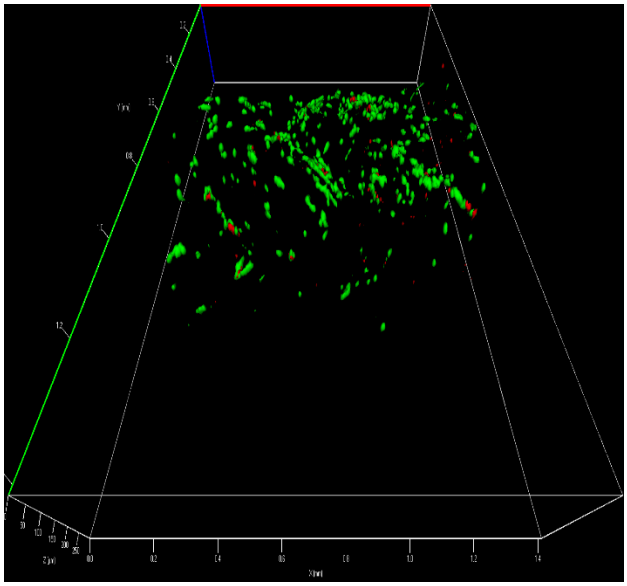

Figure 4.19 Three dimensional image of live (green) and dead (red) cells on the hollow scaffold with round fibers on Day 7

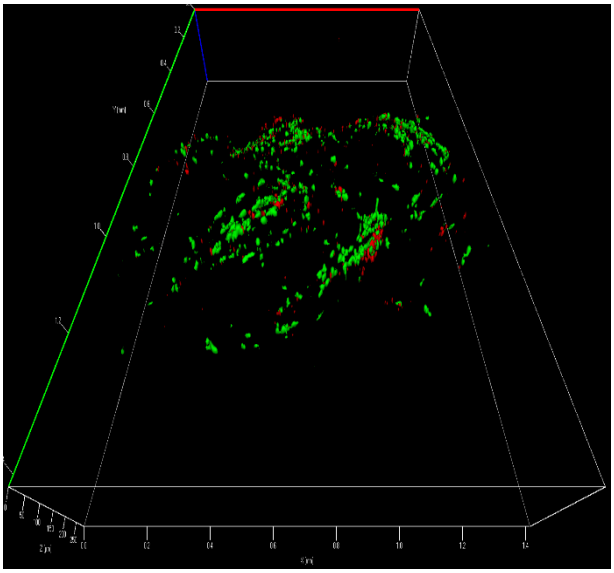

Figure 4.20 Three dimensional image of live (green) and dead (red) cells on the hollow scaffold with 4DG fibers on Day 7

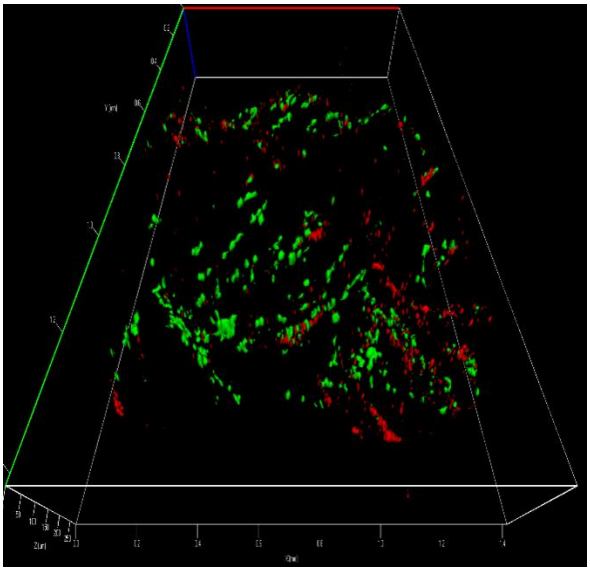

Figure 4.21 Three dimensional image of live (green) and dead (red) cells on the bilayer scaffold with 4DG fibers in the central core on Day 7

Compared to Day 3, the confocal images of the bilayer scaffold with the central core (Figures 4.18 and 4.21) show more green cells, indicating that cell migration was enhanced by including a central core within the braided structure to serve as a guidance component.

4.3.4 Quantitative polymerase chain reaction (qPCR)

Quantitative polymerase chain reaction (qPCR) was performed to evaluate the tenogenic differentiation of the sorted TGF-β Type II receptor expressing cells seeded on the three different types of scaffold for 3 weeks. This was done by checking the tenogenic markers such as scleraxis and tenomodulin. Figure 4.22 shows the relative ratio of the scleraxis protein on the three different types of scaffold and Figure 4.23 shows the relative ratio of tenomodulin on the three different types of scaffold, where

1. Uncultured Sorted TGF-β Type II receptor expressing cells

2. Sorted TGF-β Type II receptor expressing cells cultured for 3 weeks

3. Sorted TGF-β Type II receptor expressing cells on scaffold RNC cultured for 3 weeks

4. Sorted TGF-β Type II receptor expressing cells on scaffold 4DGRNC cultured for 3 weeks

5. Sorted TGF-β Type II receptor expressing cells on scaffold 4DGRC cultured for 3 weeks

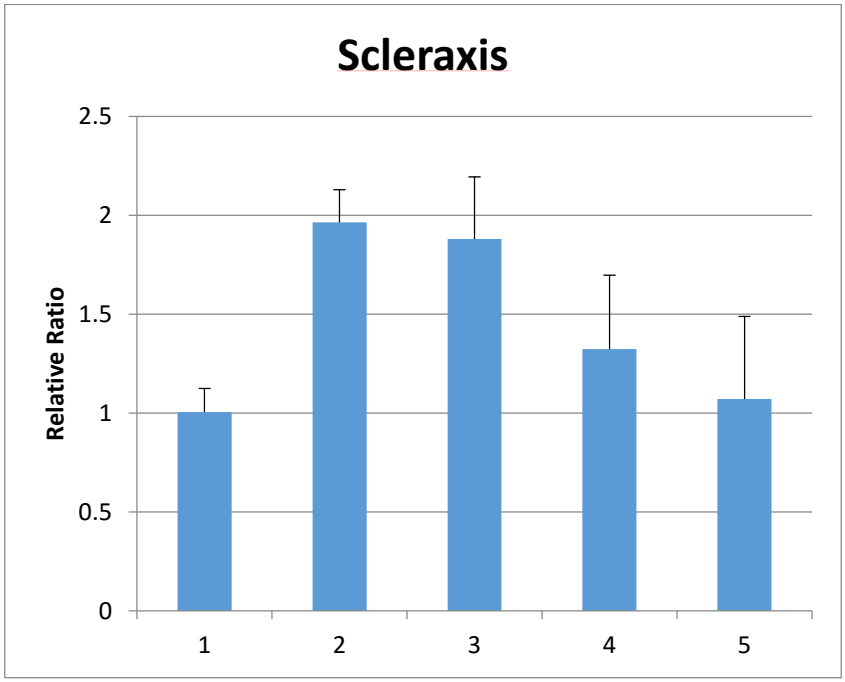

Figure 4.22 Relative ratio of the scleraxis protein on the two control samples and the three different types of scaffold

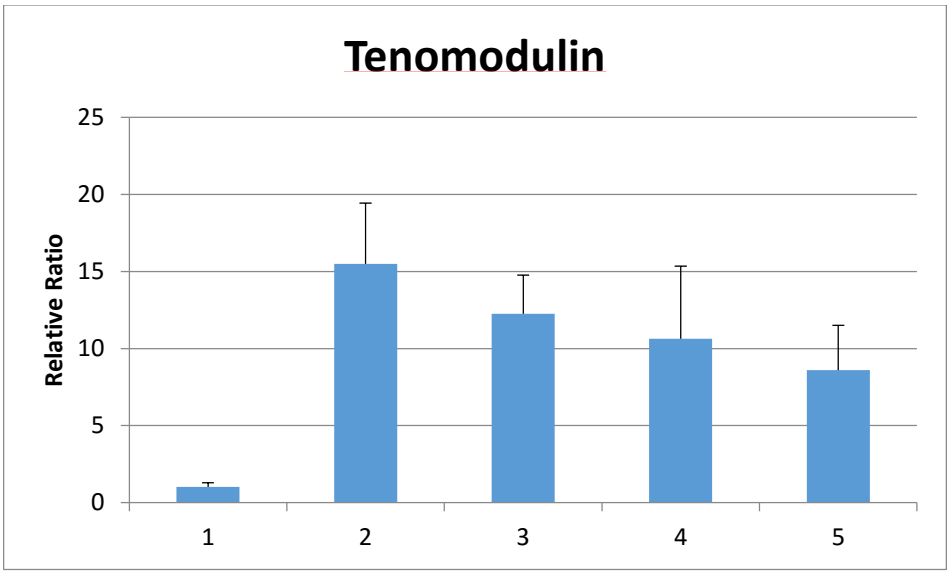

Figure 4.23 Relative ratio of tenomodulin on the two control samples and the three different types of scaffold

It can be seen that the expression of scleraxis and tenomodulin for the sorted TGF-β Type II receptor expressing cells was up-regulated by culturing the TGF-β Type II receptor expressing cells for three weeks either directly on the well plate or on the three different types of scaffolds. The levels of expression of tenomodulin were statistically higher after three weeks of culture compared to the sorted TGF-β Type II receptor expressing cells ($p \leq 0.05$). The level of expression of scleraxis on the round hollow scaffold was significantly higher than for the other two scaffolds. This result confirms that the presence of the hollow type of scaffold with round fibers increased the expression of proteins from which we can conclude that not only are the PLA fibers biocompatible with the TGF-β Type II receptor expressing cells, but that the hollow scaffold with round fibers can promote tenogenic differentiation.

The expression of tenomodulin on the hollow scaffold with round fibers was not significantly different from the cells cultured directly on the well plate ($p \geq 0.05$).

However, the gene expression of the cells cultured on the hollow scaffold with the 4DG fibers and on the bilayer scaffold with a central core containing 4DG fibers was significantly lower ($p \leq 0.05$) than when the cells were cultured directly on the well plate. This could be explained because of the lower cell seeding density leading to a lack of cell communication after seeding on the scaffolds. Total porosity and/or pore size distribution might also be an additional factors. From these observations it is proposed that the three proposed types of braided scaffolds with some improvement in their structures have the potential to be used as scaffolds for the regeneration of a tendon bone tissue junction.

Chapter 5

Conclusions and Future Work

5.1 Conclusions

As outlined in Chapter 1, the ultimate goal of this study was to develop and evaluate biodegradable multiphase scaffolds for tendon-bone junction regeneration. In summary, a series of biodegradable multiphase scaffolds was successfully fabricated from poly(lactic acid) (PLA) yarns by using a braiding technique so as to achieve the first goal of the study. In addition, the mechanical and biological evaluation of these specially designed biodegradable multiphase scaffolds has shown a satisfactory performance. The results of these mechanical and biological tests have been presented, discussed and analyzed in Chapter 4. Based on these results, the hypotheses proposed in Chapter 1 can be answered as follows.

1. The use of braiding technique has been successful in fabricating a desirable range of small pore sizes that prevent the leaking of cells into the central hollow space in the lumen of the tubular structure. Due to the interlocking structure of the braided yarns, the scaffolds acquired a porous structure which helps in cellular ingrowth and transfer of oxygen and nutrients. The pore size of the hollow scaffolds mimicking the tendon was ideal for tenocyte cell ingrowth whereas the pore size of the scaffold with the central core needed to be higher in order to facilitate osteoconduction.
2. The braided scaffolds successfully maintained their structure and avoided shrinkage during the heat setting treatment. This thermal treatment caused the poly(lactic acid) yarns to shrink and become rigid so that the braided scaffold could maintain its structural stability even in the liquid culture media during biological testing.

3. The insertion of core fibers inside the central hollow lumen of the braided structure improved the dimensional stability and tensile strength compared to the hollow scaffolds. This indicates that this multiphase structure has the ability to mimic the mechanical properties of the natural mouse bone tissue.
4. The incorporation of grooved 4DG PLA fibers marginally improved the biological properties to some extent. Although there was not much difference in proliferation and penetration of the cells between the round and the 4DG fibers, the confocal microscope images showed that the cells were attached and aligned within the grooves of the 4DG fibers as hypothesized.
5. All three types of scaffold were found to increase the expression of scleraxis and tenomodulin proteins. From this we can conclude that the PLA fibers are compatible with murine TGF β Type II receptor-expressing joint progenitor cells and have the ability to promote tenogenic differentiation.

Based on these findings for the specific hypotheses, the main conclusion of this study is that all three types of braided scaffold have the potential to be used successfully as the scaffold for the regeneration of a tendon bone junction. This study has also identified where some improvements can be made in the structure of future prototypes..

5.2 Future Work

Based on the results of this study and the literature review described in Chapter 2, there are several recommendations in terms of the structure of the scaffold and experimental design that need to be considered in order to further improve the regeneration of tendon bone junction tissue.

1. Future studies should be focused on designing hollow tubular scaffolds with both round and 4DG grooved fibers with an increased average pore size in order to promote cell migration and penetration into the scaffold. Since some of the grooves were interlocked with and covered by the round fibers during the braiding process, cells could not enter into the grooves and attach to and align along the 4DG grooved fibers. For this reason we recommend that 4DG yarns are used alone and in isolation rather than being combined with round fibers.
2. The major challenge of using murine TGF-β Type II receptor-expressing joint progenitor cells is to be able to generate a sufficient quantity of positive cells following cell-sorting. We found that there were significantly more TGF-β Type II negative cells than positive ones. This led to some cell culturing trials where insufficient numbers of cells (i.e. less than 10^5) were seeded per well, which led to an unsuccessful outcome in terms of viability and migration. In future, additional mice embryos will be needed in order to generate sufficient numbers of positive TGF-β Type II cells.
3. In this study the PLA scaffolds were coated in fetal bovine serum prior to cell seeding so as to improve their cytocompatibility. We recommend that other surface treatments be considered. For example, it would be interesting to determine whether coating the PLA scaffolds with Type 1 collagen or fibronectin would improve cell attachment, viability, proliferation and gene expression of murine TGF- β Type II receptor-expressing joint progenitor cells.
4. In order to increase the rate and extent of cell migration and differentiation, mechanical stimulation should be applied to the scaffolds in the axial direction during cell culture.

5. *In vivo* animal studies and clinical trials are very important and necessary to evaluate the clinical capability of the specially designed scaffolds for regeneration of tendon bone junction tissue. It is important to study their handling, implantation, healing, tissue regeneration and immune response when placed inside the human body.

REFERENCES

1. Summers, A. P., & Koob, T. J. (2002). The evolution of tendon—morphology and material properties. *Comparative Biochemistry and Physiology Part A: Molecular & Integrative Physiology*, *133*(4), 1159-1170.
2. Wang, J. H. C. (2006). Mechanobiology of tendon. *Journal of Biomechanics*,*39*(9), 1563-1582.
3. Ker, R. F. (2007). Mechanics of tendon, from an engineering perspective .*International Journal of Fatigue*, *29*(6), 1001-1009.
4. Lin, T. W., Cardenas, L., & Soslowsky, L. J. (2004). Biomechanics of tendon injury and repair. *Journal of Biomechanics*, *37*(6), 865-877.
5. Silver, F. H., Freeman, J. W., & Seehra, G. P. (2003). Collagen self-assembly and the development of tendon mechanical properties. *Journal of Biomechanics*, *36*(10), 1529-1553.
6. Wren, T. A., Yerby, S. A., Beaupré, G. S., & Carter, D. R. (2001). Mechanical properties of the human Achilles tendon. *Clinical Biomechanics*, *16*(3), 245-251.
7. Yang, G., Rothrauff, B. B., & Tuan, R. S. (2013). Tendon and ligament regeneration and repair: clinical relevance and developmental paradigm. *Birth Defects Research Part C: Embryo Today: Reviews*, *99*(3), 203-222.
8. Apostolakos, J., Durant, T. J., Dwyer, C. R., Russell, R. P., Weinreb, J. H., Alaee, F., ... & Mazzocca, A. D. (2014). The enthesis: a review of the tendon-to-bone insertion. *Muscles, Ligaments and Tendons Journal*, *4*(3), 333.

9. Benjamin, M., Toumi, H., Ralphs, J. R., Bydder, G., Best, T. M., & Milz, S. (2006). Where tendons and ligaments meet bone: attachment sites ('entheses') in relation to exercise and/or mechanical load. *Journal of Anatomy*, *208*(4), 471-490.
10. Bunker, D. L. J., Ilie, V., Ilie, V., & Nicklin, S. (2014). Tendon to bone healing and its implications for surgery. *Muscles, Ligaments and Tendons Journal*, *4*(3), 343.
11. Thomopoulos, S., Genin, G. M., & Galatz, L. M. (2010). The development and morphogenesis of the tendon-to-bone insertion What development can teach us about healing. *Journal of Musculoskeletal & Neuronal Interactions*, *10*(1), 35.
12. Thomopoulos, S., Williams, G. R., Gimbel, J. A., Favata, M., & Soslowsky, L. J. (2003). Variation of biomechanical, structural, and compositional properties along the tendon to bone insertion site. *Journal of Orthopaedic Research*, *21*(3), 413-419.
13. Waggett, A. D., Ralphs, J. R., Kwan, A. P., Woodnutt, D., & Benjamin, M. (1998). Characterization of collagens and proteoglycans at the insertion of the human Achilles tendon. *Matrix Biology*, *16*(8), 457-470.
14. Genin, G. M., Kent, A., Birman, V., Wopenka, B., Pasteris, J. D., Marquez, P. J., & Thomopoulos, S. (2009). Functional grading of mineral and collagen in the attachment of tendon to bone. *Biophysical Journal*, *97*(4), 976-985.
15. Thomopoulos, S., Marquez, J. P., Weinberger, B., Birman, V., & Genin, G. M. (2006). Collagen fiber orientation at the tendon to bone insertion and its influence on stress concentrations. *Journal of Biomechanics*, *39*(10), 1842-1851.
16. Vanderby, R., &Provenzano, P. P. (2003). Collagen in connective tissue: from tendon to bone. *Journal of Biomechanics*, *36*(10), 1523-1527.

17. Thomopoulos, S., Marquez, J. P., Weinberger, B., Birman, V., & Genin, G. M. (2006). Collagen fiber orientation at the tendon to bone insertion and its influence on stress concentrations. *Journal of Biomechanics*, *39*(10), 1842-1851.
18. Rufai, A., Ralphs, J. R., & Benjamin, M. (1995). Structure and histopathology of the insertional region of the human Achilles tendon. *Journal of Orthopaedic Research*, *13*(4), 585-593.
19. Petersen, W., & Laprell, H. (2000). Insertion of autologous tendon grafts to the bone: a histological and immunohistochemical study of hamstring and patellar tendon grafts. *Knee Surgery, Sports Traumatology, Arthroscopy*, *8*(1), 26-31.
20. Smith, L., Xia, Y., Galatz, L. M., Genin, G. M., & Thomopoulos, S. (2012). Tissue-engineering strategies for the tendon/ligament-to-bone insertion. *Connective Tissue Research*, *53*(2), 95-105.
21. Achilles Tendon Information - Achilles Tendon. (n.d.). Retrieved 2015, from http://achillestendon.com/achilles-tendon-information/
22. Normal knee anatomy: MedlinePlus Medical Encyclopedia Image. (n.d.). Retrieved 2015, from http://www.nlm.nih.gov/medlineplus/ency/imagepages/8716.htm
23. Lu, H. H., Subramony, S. D., Boushell, M. K., & Zhang, X. (2010). Tissue engineering strategies for the regeneration of orthopedic interfaces. *Annals of Biomedical Engineering*, *38*(6), 2142-2154.
24. Spalazzi, J. P., Dagher, E., Doty, S. B., Guo, X. E., Rodeo, S. A., & Lu, H. H. (2008). In vivo evaluation of a multiphased scaffold designed for orthopaedic interface tissue

engineering and soft tissue-to-bone integration. *Journal of Biomedical Materials Research Part A, 86*(1), 1-12.

25. Yang, P. J., &Temenoff, J. S. (2009). Engineering orthopedic tissue interfaces. *Tissue Engineering Part B: Reviews*, *15*(2), 127-141.
26. Liu, Y. X., Thomopoulos, S., Birman, V., Li, J. S., &Genin, G. M. (2012). Bi-material attachment through a compliant interfacial system at the tendon-to-bone insertion site. *Mechanics of Materials*, *44*, 83-92.
27. Chen, C. H., Chang, C. H., Wang, K. C., Su, C. I., Liu, H. T., Yu, C. M., ... & Liu, H. W. (2011). Enhancement of rotator cuff tendon–bone healing with injectable periosteum progenitor cells-BMP-2 hydrogel in vivo. *Knee Surgery, Sports Traumatology, Arthroscopy*, *19*(9), 1597-1607.
28. Shahab-Osterloh, S., Witte, F., Hoffmann, A., Winkel, A., Laggies, S., Neumann, B., ...& Gross, G. (2010). Mesenchymal Stem Cell-Dependent Formation of Heterotopic Tendon-Bone Insertions (Osteotendinous Junctions).*Stem Cells*, *28*(9), 1590-1601.
29. Zhang, J., & Wang, J. H. (2014). Kartogenin induces cartilage-like tissue formation in tendon–bone junction. *Bone Research, 2*.
30. Nakase, J., Kitaoka, K., Matsumoto, K., & Tomita, K. (2010). Facilitated tendon-bone healing by local delivery of recombinant hepatocyte growth factor in rabbits. *Arthroscopy: The Journal of Arthroscopic & Related Surgery*, *26*(1), 84-90.
31. Nourissat, G., Diop, A., Maurel, N., Salvat, C., Dumont, S., Pigenet, A., ...&Berenbaum, F. (2010). Mesenchymal stem cell therapy regenerates the native bone-tendon junction

after surgical repair in a degenerative rat model. *Public Library of Science One, 5(8),* 1-11.

32. Kanazawa, T., Soejima, T., Noguchi, K., Tabuchi, K., Noyama, M., Nakamura, K. I., & Shiba, N. (2014). Tendon-to-bone healing using autologous bone marrow-derived mesenchymal stem cells in ACL reconstruction without a tibial bone tunnel-A histological study. *Muscles, Ligaments and Tendons Journal*, *4*(2), 201.
33. Chang, C. H., Chen, C. H., Su, C. Y., Liu, H. T., & Yu, C. M. (2009). Rotator cuff repair with periosteum for enhancing tendon–bone healing: a biomechanical and histological study in rabbits. *Knee Surgery, Sports Traumatology, Arthroscopy*, *17*(12), 1447-1453.
34. Hashimoto, Y., Yoshida, G., Toyoda, H., & Takaoka, K. (2007). Generation of tendon-to-bone interface "enthesis" with use of recombinant BMP-2 in a rabbit model. *Journal of Orthopaedic Research*, *25*(11), 1415-1424.
35. Ide, J., Kikukawa, K., Hirose, J., Iyama, K. I., Sakamoto, H., Fujimoto, T., & Mizuta, H. (2009). The effect of a local application of fibroblast growth factor-2 on tendon-to-bone remodeling in rats with acute injury and repair of the supraspinatus tendon. *Journal of Shoulder and Elbow Surgery*, *18*(3), 391-398.
36. Kadonishi, Y., Deie, M., Takata, T., & Ochi, M. (2012). Acceleration of tendon–bone healing in anterior cruciate ligament reconstruction using an enamel matrix derivative in a rat model. *Journal of Bone & Joint Surgery, British Volume*, *94*(2), 205-209.
37. Yokoya, S., Mochizuki, Y., Nagata, Y., Deie, M., & Ochi, M. (2008). Tendon-bone insertion repair and regeneration using polyglycolic acid sheet in the rabbit rotator cuff injury model. *The American Journal of Sports Medicine*, *36*(7), 1298-1309.

38. Gupta, B., Revagade, N., & Hilborn, J. (2007). Poly (lactic acid) fiber: an overview. *Progress in Polymer Science*, *32*(4), 455-482.
39. Lunt, J. (1998). Large-scale production, properties and commercial applications of polylactic acid polymers. *Polymer Degradation and Stability*, *59*(1), 145-152.
40. Mehta, R., Kumar, V., Bhunia, H., & Upadhyay, S. N. (2005). Synthesis of poly (lactic acid): a review. *Journal of Macromolecular Science, Part C: Polymer Reviews*, *45*(4), 325-349.
41. Lim, L. T., Auras, R., & Rubino, M. (2008). Processing technologies for poly (lactic acid). *Progress in Polymer Science*, *33*(8), 820-852.
42. Mathur, M., & Hira, M. A. (2008). Specialty Fibres-IV: Poly Lactic Acid Fibres. *Man-Made Textiles in India*, *51*(7).
43. Dugan, J. S. (2001). Novel properties of PLA fibers. *International Nonwovens Journal*, *10*(3), 29-33.
44. Ouyang, H. W., Goh, J. C., Thambyah, A., Teoh, S. H., & Lee, E. H. (2003). Knitted poly-lactide-co-glycolide scaffold loaded with bone marrow stromal cells in repair and regeneration of rabbit Achilles tendon. *Tissue Engineering*, *9*(3), 431-439.
45. Spagnoli, A., O'Rear, L., Chandler, R. L., Granero-Molto, F., Mortlock, D. P., Gorska, A. E., ...& Moses, H. L. (2007). TGF-β signaling is essential for joint morphogenesis. *The Journal of Cell Biology*, *177*(6), 1105-1117.
46. Li, T., Longobardi, L., Myers, T. J., Temple, J. D., Chandler, R. L., Ozkan, H., ...& Spagnoli, A. (2012). Joint TGF-β type II receptor-expressing cells: ontogeny and characterization as joint progenitors. *Stem Cells and Development*, *22*(9), 1342-1359.

47. ASTM International, (2010), *ASTM F2450-10 Standard Guide for Assessing Microstructure of Polymeric Scaffolds for Use in Tissue Engineered Medical Products*, ASTM International

48. ASTM International, (2011), *ASTM D5035-11 Standard Test Method for Breaking Force and Elongation of Textile Fabrics (Strip Method)*, ASTM International

49. Markaki, A. E. (2009). AlamarBlue® Assay for Assessment of Cell Proliferation using the FLUOstar OPTIMA. *BMG Lab Tech*.

50. Docheva, D., Hunziker, E. B., Fässler, R., &Brandau, O. (2005). Tenomodulin is necessary for tenocyte proliferation and tendon maturation. *Molecular and Cellular Biology*, *25*(2), 699-705.

51. Dhandayuthapani, B., Yoshida, Y., Maekawa, T., & Kumar, D. S. (2011). Polymeric scaffolds in tissue engineering application: a review. *International Journal of Polymer Science*, *2011*.

52. Yamada, H., & Evans, F. G. (1970). *Strength of Biological Materials*, Robert E. Krieger Publishing Co.: Huntington, NY.

53. Garlotta, D. (2001). A literature review of poly (lactic acid). *Journal of Polymers and the Environment*, *9*(2), 63-84.

54. Cserjesi, P., Brown, D., Ligon, K. L., Lyons, G. E., Copeland, N. G., Gilbert, D. J., ... & Olson, E. N. (1995). Scleraxis: a basic helix-loop-helix protein that prefigures skeletal formation during mouse embryogenesis. *Development*,*121*(4), 1099-1110.

55. Rebouças, E. D. L., Costa, J. J. D. N., Passos, M. J., Passos, J. R. D. S., Hurk, R. V. D., & Silva, J. R. V. (2013). Real time PCR and importance of housekeeping genes for

normalization and quantification of mRNA expression in different tissues. *Brazilian Archives of Biology and Technology*, *56*(1), 143-154.

56. Braid and Shield Calculations. (n.d.). Retrieved (2015), from http://www.cmcorporation.com/cable-and-shielding-information/braid-and-shield-calculations